Predicting elastic modulus degradation of alkali silica reaction affected concrete using soft computing techniques: a comparative study

Yang Yu [a,*], Thuc N. Nguyen [a], Jianchun Li [a,*], Leandro F.M. Sanchez [b], Andy Nguyen [c]

[a] Centre for Built Infrastructure Research (CBIR), University of Technology Sydney, Sydney, NSW, Australia

[b] Department of Civil Engineering, University of Ottawa, Ottawa, ON, Canada

[c] School of Civil Engineering and Surveying, University of Southern Queensland, Springfield, Australia

Abstract: Alkali silica reaction (ASR) is a harmful distress mechanism which results in expansion and reduction of mechanical properties of concrete. The latter may cause loss of serviceability and load carrying capacity of affected concrete structures. Influences of ASR on concrete are known to be complex in nature, for which the traditional empirical and curve-fitting approaches are insufficient to provide adequate models to capture such complexity. Recent advancement in soft computing (SC) offers a new tool for tackling the complexity of ASR affected concrete. Most of previous experimental studies agreed that as a result of ASR, the elastic modulus suffers a significant reduction compared with other properties such as compressive and tensile strength of the affected concrete. In this study, an investigation has been conducted, utilising different SC models to quantify ASR-induced elastic modulus degradation of unrestrained concrete. Five SC techniques, namely support vector machine (SVM), artificial neural network (ANN), adaptive neuro-fuzzy inference system (ANFIS), M5P model and genetic expression programming (GEP), are investigated comparatively in this research. The models, on basis of SC techniques, are developed and tested using a comprehensive dataset collected from existing publications. In order to demonstrate the superiorities of SC techniques, the proposed approaches are compared to several empirical models developed using same dataset. The comparative results show that the developed SC models outperform empirical models in a wide range of evaluation indices, which indicates promising applications of the proposed approach.

Keywords: Alkali silica reaction (ASR), Concrete, Elastic modulus, Support vector machine, Artificial neural network, Adaptive neuro-fuzzy inference system, M5P, Genetic expression programming

1. Introduction

Alkali silica reaction (ASR) is one of major research challenges in the field of concrete durability and may reduce the lifetime of affected concrete structures and increase the maintenance cost meanwhile [1, 2]. To assess

* Corresponding authors.
E-mail addresses: yang.yu@uts.edu.au (Y. Yu), jianchun.li@uts.edu.au (J. Li)

the effects of ASR on the behaviour of concrete materials and structures, plenty of experimental investigations have been carried out to investigate the changes of mechanical properties of concrete as a function of ASR development. Sanchez et al. evaluated the mechanical performance of ASR-affected concrete specimens presenting 3 distinct strengths and including a broad range of reactive aggregates [4]. The testing results showed that the reductions in tensile strength and elastic modulus were higher than that of compressive strength. The latter was found to be related to the microscopic distress features of ASR affected concrete [4]. Kubo and Nakara tested the mechanical properties of concrete specimens with 3 sorts of reactive aggregates in Japan [5]. The results demonstrated a similar observation of insignificant change in compressive strength due to ASR, while the loss in the elastic modulus was more obvious. In another research, Giaccio et al. studied the mechanical behaviour of ASR-affected concrete with three types of reactive aggregates: reactive siliceous orthoquartzite, natural reactive sand and slow reactive granitic [6]. The comparison results showed that compared with compressive and splitting tensile strengths, the elastic modulus is more sensitive to ASR and can be considered as the optimal index to identify the progression of ASR in concrete. Based on the above experimental results, constitutive relationships between the loss in concrete mechanical properties and ASR-induced expansion were investigated and a variety of empirical models have been subsequently developed to predict the change of mechanical properties due to ASR. However, the existing models were developed based on the expansion level only, while other important factors such as mix-proportion, reactive aggregate type, alkali content and external environmental conditions that can directly affect ASR development were not considered. For this reason, the empirical models may fail to predict the losses of mechanical properties of different specimens when these factors are varied. Consequently, it is definitely necessary to develop robust models considering all the influence factors to accurately the mechanical properties of a range of ASR-affected concrete.

Currently, soft computing (SC) approaches are being widely developed and utilized to solve various engineering problems in the field of concrete, which shows the effectiveness in describing complicated and highly nonlinear relationships between a large number of input variables and output targets. For example, Getahun et al. employed artificial neural networks (ANN) to evaluate 28-day splitting tensile and compressive strengths of the concrete with reclaimed asphalt pavement and rice husk ash as partial substitute of virgin aggregates and Portland cement (PC) [7]. Yaseen et al. adopted extreme learning machine (ELM) to design a numerical model to predict compressive strength of lightweight foamed concrete, in which PC content, ratio of water to binder, oven dry density and foam volume are used as model inputs [8]. Sonebi et al. used the support vector machine (SVM) to characterize fresh properties of self-computing concrete. In that research, the capacities of two SVM-based predictive models with different types of kernels (polynomial function and radial basis function) were investigated. In another work, Sadrossadat et al. studied the performance of the gene expression programming (GEP) method to forecast confined compressive strength and corresponding strain of reinforced concrete (RC) circular columns. The GEP-based model was also developed for the mix-design of lightweight concrete [11]. In addition, Basarir et al. utilized adaptive neuro-fuzzy inference systems (ANFIS) to model ultimate pure bending moment of cold-formed and fabricated tubes filled with concrete, the superiority of which was also illustrated via a comparison with linear and nonlinear multiple regression models [12]. Elastic modulus and compressive strength of recycled aggregate concrete were evaluated using M5P model tree algorithms [13, 14]. Based on excellent prediction results in above studies, SC techniques are proven to be a potential solution to take into consideration of several influential factors in predicting the reduction of ASR-induced mechanical properties. To the best knowledge of authors, application of SC methods in predicting mechanical properties of ASR-affected concrete is rarely reported.

In this study, five SC techniques are first explored to develop nonlinear predictive models to quantify the elastic modulus change of ASR-affected concrete under free-expansion, which include ANN, SVM, ANFIS, M5P tree and GEP. To enhance the generalization ability of developed models, different optimization and training algorithms are employed to adjust the best model architectures. The performances of the proposed SC models are appraised by a comprehensive database consisting of test data collected from existing studies. To demonstrate the superiorities of the proposed models, they are compared to the empirical models that are most commonly used in practice. Finally, a user-friendly graphical user interface (GUI) software is developed to assist engineers to better handle these SC models in evaluating the mechanical performance of ASR-affected concrete material and structures in practice.

2. Overview of the proposed soft computing techniques

2.1. Artificial neural network

Artificial neural network (ANN) is a type of distributed parallel information processing mathematical models that simulate the neurobehavioral characteristics of animals [16, 17]. Relying on the system complexity, ANN is able to adjust the relationship among a large number of internal neurons to achieve information processing. Among existing ANN models, the back propagation neural network (BPNN) is most widely utilised in engineering applications. The training of BPNN is based on error inverse propagation algorithm, the procedure of which includes forward information propagation and back error propagation. Generally, the BPNN consists of an input layer, a or several hidden layers and an output layer. Fig. 1 gives an example of BPNN with configuration of *p* input neuron, a hidden layer with *q* neurons and an output neuron. The input and output relationship of *j*th hidden neuron could be represented as follows:

$$Op1_j = \sum_{i=1}^{p} x_i\, w_{i,j} + b_j \tag{1}$$

$$y_j = f_t(Op1_j) \tag{2}$$

where y_j denotes the output of *j*th hidden neuron; x_i denotes *i*th input of the hidden neuron; $w_{i,j}$ denotes the weight of connection between *i*th input neuron and *j*th hidden neuron; b_j denotes the bias at *j*th hidden neuron; f_t denotes transfer function. Then, all the outputs at hidden neurons are regarded as the inputs for the output layer. The output of BPNN can be shown in Eqs. (3) and (4):

$$Op2 = \sum_{j=1}^{q} y_j\, v_j + b_o \tag{3}$$

$$Y_{out} = f_t(Op2) \tag{4}$$

where Y_{out} denotes the output of the BPNN; v_j denotes the connection weight between *j*th hidden neuron and output neuron; b_o denotes the bias at output neuron.

The training of the BPNN is to use the BP algorithms to regulate the values of connection weights and bias to achieve the best performance. The optimisation objective is the mean square error between network outputs and practical expectations of training samples. The mathematical expression of cost function is given in Eq. (5):

$$H_{mse} = \frac{1}{N_s} \sum_{k=1}^{N_s} [Y_{out}(k) - y_p(k)]^2 \tag{5}$$

where y_p denotes the practical output value of *i*th training sample and N_s denotes the total number of training samples.

Supposing that the relationship between network inputs and output are monotonous, the effect of *i*th input on the network output can be obtained via calculating the partial derivative of the output Y_{out} relative to *i*th input x_i, the expression of which is given as follows:

$$E_i = \frac{\partial Y_{out}}{\partial x_i} = \sum_{j=1}^{q} \frac{\partial Y_{out}}{\partial Op2} \frac{\partial Op2}{\partial y_j} \frac{\partial y_j}{Op1_j} \frac{Op1_j}{\partial x_i} = \sum_{j=1}^{q} [f_t'(Op2) v_j f_t'(Op1_j) w_{i,j}] \tag{6}$$

In Eq. (6), $f_t'(Op2)$ and $f_t'(Op1_j)$ are supposed to be constants. As a result, the input x_i with high negative or positive value of E_i has more negative or positive effect on the network output Y_{out}.

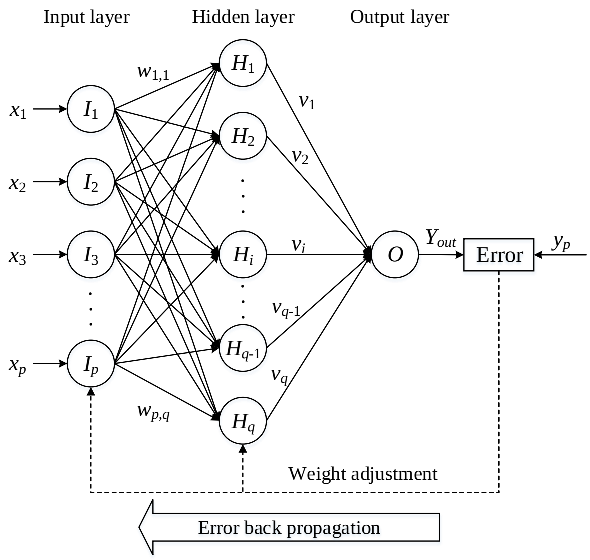

Fig. 1. Configuration of a three-layer BP neural network

2.2. Support vector machine

Support vector machine (SVM) is capable of achieving small sample, nonlinear and high-dimensional pattern recognition [18, 19]. By introducing insensitive loss function ε, SVM can also be utilised to solve the regression fitting problems. The main principle of the SVM is that it uses the kernel function to map linear indivisible problem in low-dimensional space into linear divisible problem in high-dimensional space. Suppose a dataset $D=\{(x_i, y_i), i=1, 2, \ldots, l\}$, where (x_i, y_i) denotes input and output pair of ith sample. The regression function is provided as follows:

$$f(x) = \omega^T \varphi(x) + b \tag{7}$$

where ω denotes weight vector, $\varphi(x)$ denotes nonlinear mapping between low-dimensional feature space and high-dimensional feature space, and b denotes threshold value. Then, a structural risk function is introduced:

$$R_{reg} = \frac{1}{2}\|\omega\|^2 + C \cdot \frac{1}{n}\sum_{i=1}^{n}|y_i - f(x_i)| \tag{8}$$

where $\|\omega\|^2$ denotes the description function. C denotes the penalty parameter. $|y_i - f(x_i)|$ denotes the ε-insensitive loss function, as illustrated in Fig. 2. The following equation is corresponding expression:

$$|y - f(x)| = \begin{cases} |y - f(x)| - \varepsilon, & |y - f(x)| > \varepsilon \\ 0, & |y - f(x)| \le \varepsilon \end{cases} \tag{9}$$

Solving regression problem above is equivalent to minimising the following cost function:

$$\min\ \frac{1}{2}\|\omega\|^2 + C\sum_{i=1}^{n}(\xi_i + \xi_i^*)$$

$$s.t.\ y_i - \omega^T\varphi(x_i) - b \le \varepsilon + \xi_i^*, i = 1,2,\ldots,n \tag{10}$$

$$y_i - \omega^T\varphi(x_i) - b \le \varepsilon + \xi_i, i = 1,2,\ldots,n$$

$$\xi_i,\ \xi_i^* \geq 0, i = 1,2,\dots,n$$

where ξ_i and ξ_i^* are slack variables and ε denotes the insensitive loss factor, which is employed to control the amplitude of regression approximation error. To solve such an optimisation problem, the Lagrange function is introduced and the following function can be obtained using Karush-Kuhn-Tucker (KKT) conditions:

$$f(x) = \sum_{i=1}^{n}(a_i + a_i^*)K(x_i, x) + b \tag{11}$$

where a_i and a_i^* are Lagrange multipliers. $K(x_i, x) = \varphi(x_i) \cdot \varphi(x)$ is kernel function satisfying the Mercer condition. In this work, the radial basis function is considered due to good nonlinear prediction ability, the mathematical expression of which is given as follows:

$$K(x_i, x) = \exp(-\frac{\|x_i - x\|^2}{2\sigma^2}) \tag{12}$$

where σ is kernel function parameter. Substituting Eq. (12) into Eq. (11), the regression function can be expressed as follows:

$$f(x) = \sum_{i=1}^{n}(a_i + a_i^*)\exp(-\frac{\|x_i - x\|^2}{2\sigma^2}) + b \tag{13}$$

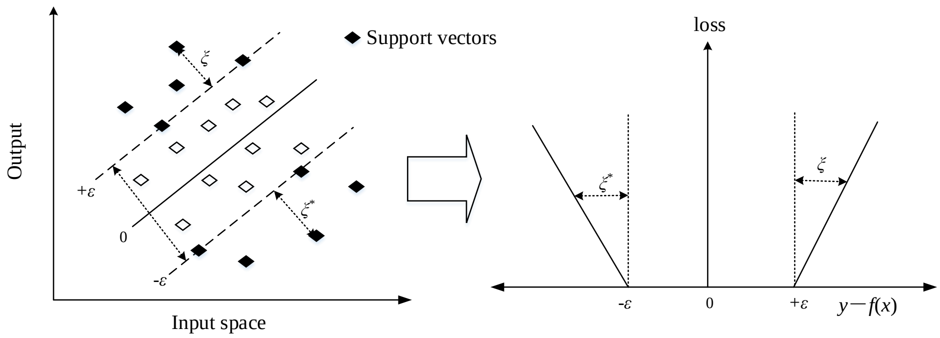

Fig. 2. ε-insensitive loss function.

2.3. Adaptive neuro-fuzzy inference system

Adaptive neuro-fuzzy inference system (ANFIS) is a hybrid smart system, combining the benefits of learning algorithms of ANN and fuzzy inference mechanism to achieve nonlinear mapping between inputs and outputs [20, 21]. Compared with conventional fuzzy inference systems, the ANFIS has stronger self-learning ability and adaptability, which is being broadly applied in a variety of engineering fields. In ANFIS, the Sugeno fuzzy model is employed to build up fuzzy IF-THEN rules. The principle of ANFIS is that based on a given group of input-output data pairs, a fuzzy inference system is established and trained via adaptive adjustment of the parameters of membership functions. Generally, the ANFIS model is composed of a set of directly connected neurons and each of them can be considered as a processing unit to generate an output. Fig. 3 shows a simple example of ANFIS architecture with *m* inputs, one output and *u* fuzzy rules. The detailed descriptions of fuzzy rules are provided as follows:

Rule 1: if x_1 is $A_{1,1}$ and x_2 is $A_{1,2}$, …, and x_m is $A_{1,m}$, then $y=a_{1,0}+a_{1,1}x_1+a_{1,2}x_2+\cdots+a_{1,m}x_m$

Rule 2: if x_1 is $A_{2,1}$ and x_2 is $A_{2,2}$, …, and x_m is $A_{2,m}$, then $y=a_{2,0}+a_{2,1}x_1+a_{2,2}x_2+\cdots+a_{2,m}x_m$

⋮

Rule *u*: if x_1 is $A_{u,1}$ and x_2 is $A_{u,2}$, …, and x_m is $A_{u,m}$, then $y=a_{u,0}+a_{u,1}x_1+a_{u,2}x_2+\cdots+a_{u,m}x_m$

where $x_1, x_2,\ldots, x_m$ are the system inputs; y denotes the system output; $a_{1,0}, \ldots, a_{1,m}, a_{2,0}, \ldots, a_{2,m},\ldots, a_{u,0}, \ldots, a_{u,m}$ are constants; $A_{1,1}, \ldots, A_{1,m}, A_{2,1}, \ldots, A_{2,m},\ldots, A_{u,1}, \ldots, A_{u,m}$ denote the membership functions of the antecedent part. In this paper, the Gaussian function is employed to represent $A_{i,k}$ (i=1,…,u, k=1,…,m) and its expression is shown in Eq. (14):

$$A_{i,k}(x_k) = \exp[-\frac{(x_k-\mu_{i,k})^2}{\delta_{i,k}^2}] \tag{14}$$

where $\delta_{i,k}$ and $\mu_{i,k}$ denote the deviation and mean, respectively.

As can be seen from Fig. 3, the ANFIS is a five-layer neural network. The first layer is fuzzified layer, which consists of $u\cdot m$ neurons. The function of this layer is to fuzzify input variables and calculate the membership values of input data to the fuzzy set. The output of this layer can be expressed as follows:

$$O_{i,k}^1 = A_{i,k}(x_k) \tag{15}$$

The second layer is rule inference layer, which has one neuron for each fuzzy rule. In rule inference layer, firing strength of each fuzzy rule is calculated via multiplying the membership values at that rule, the expression of which is shown in Eq. (16):

$$O_i^2 = \prod_{k=1}^m O_{i,k}^1 \tag{16}$$

The third layer is normalisation layer, which has one neuron corresponding to each fuzzy rule. In normalisation layer, firing strength of each rule is normalised using the following equation to signify its contribution to final result:

$$O_i^3 = \frac{O_i^2}{\sum_{i=1}^u O_i^2} \tag{17}$$

The fourth layer is defuzzification layer, where one neuron corresponds to each fuzzy rule. In this layer, the result of each rule can be obtained using Eq. (18):

$$O_i^4 = O_i^3 \cdot (a_{u,0} + a_{i,1}x_1 + a_{i,2}x_2 + \cdots + a_{i,m}x_m) \tag{18}$$

The fifth layer is output layer that generates final output of ANFIS via summarising the result of each fuzzy rule. The mathematical expression is shown in Eq. (19):

$$O_i^5 = \sum_{i=1}^u O_i^4 \tag{19}$$

In the ANFIS, the parameters $\delta_{i,k}$, $\mu_{i,k}$, $a_{1,0}$, …, $a_{u,m}$ (i=1,…,u, k=1,…,m) could be adjusted to realise best network performance. In this study, a hybrid method on basis of gradient descent (GD) and least square method is used to identify these parameters, the procedure of which include forward passing and back propagation. In the forward passing learning process, the parameters $\delta_{i,k}$ and $\mu_{i,k}$ are fixed and least square method is applied to identify the values of $a_{1,0}$, …, $a_{u,m}$. In the forward propagation learning process, $a_{1,0}$, …, $a_{u,m}$ are fixed and the GD method is adopted to update the values of $\delta_{i,k}$ and $\mu_{i,k}$.

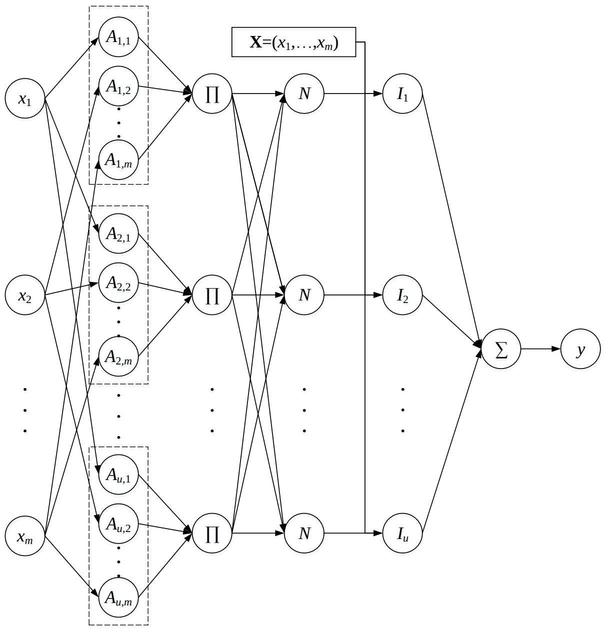

Fig. 3. Typical configuration of ANFIS.

2.4. M5P model

M5 model, proposed by Quinlan, is a type of segmented multiple liner regression tree model [22]. The principle of M5 model is to separate the data space into a group of sub-spaces and then set up model tree in each sub-space where the information can be extracted. Fig. 4 depicts an example of M5 model where the data space is divided into four sub-spaces.

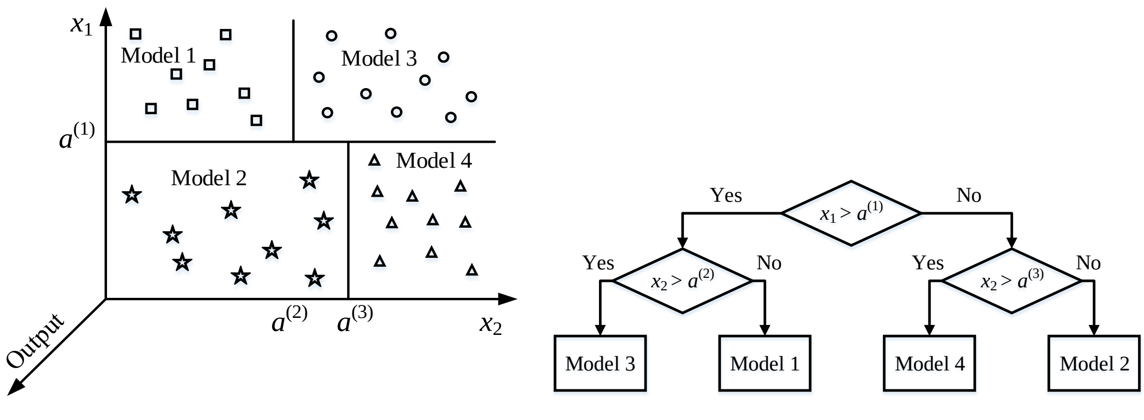

(a) (b)

Fig. 4. Schematic of M5 model, (a) input separation; (b) model construction.

M5P model is an extension of M5 model, which aims at refining the data space based on the principle of sample attribute difference. When the sample number at some node is less than a certain value or the standard deviation of sample attributes is less than a certain limit, the space splitting is finished. Here, the sample attribute difference is expressed by standard deviation reduction (SDR) factor, the expression of which is given as follows:

$$SDR = sd(M) - \sum_k \frac{M_k}{|M|} \cdot sd(M_k) \tag{20}$$

where M denotes the total set of sampling arriving at some node; M_k denotes kth sample set in kth sub-space separated from M; $sd(M_k)$ denotes the attribute standard deviation of sample set M_k. This procedure is equivalent to that of tree growth simulation. After all the samples are refined, an initial model tree will be generated. The node where the model tree stops growing is called the leaf sub-node. For the samples at the leaf sub-node, linear regression algorithm is employed to generate a multivariate regression equation. Finally, the linear model is obtained.

To enhance the application efficiency of whole model, it is necessary to transverse each node at initial model tree via the pruning process. Some sub-trees are merged and replaced with leaf nodes. To start with, linear regression algorithm is used to fit the multivariate linear equation of the node. Then, the reduction of prediction error is used as the pruning criteria to decide whether the sub-tree of the node should be retained, which can be expressed as follows:

$$E_R = |N|RMSE - |N_l|RMSE_l - |N_r|RMSE_r \tag{21}$$

where $RMSE$ denotes the root mean square (RMS) error of fitting equation predictions at some node; $RMSE_l$ and $RMSE_r$ denote RMS errors of predictions at left and right sub-nodes of this node. When the value of E_R is positive, this sub-tree is retained. Otherwise, it will be changed to a leaf sub-node.

After the pruning recursive process, the initial model tree is optimised into a model tree with the simplest structure. However, linear models of adjacent leaf sub-nodes in the model tree may generate the discontinuity, which will lead to the nonlinearity at the section points and affect model prediction accuracy. To fix this problem, in the model tree smoothing process two multivariate linear fitting equations of child node and parent node of each node can be merged into a new linear equation, shown as follows:

$$f_r = \frac{lf_s + cf_d}{l + c} \tag{22}$$

where f_s denotes the fitting equation of child node; f_d denotes the fitting equation of parent node; f_r denotes the new equation; l is the number of samples arriving at the node; c is a constant and $c = 15$ in this paper. When the change of RMSE is less than a pre-set threshold, the linear equation of the node is replaced with new equation. Otherwise, keep linear equation unchanged.

2.5. Gene expression programming

The gene programming (GP) was proposed by Koza, which is a novel heuristic algorithm on basis of the principle of genetics and biological evolution in nature [23]. It is the extension of genetic algorithm (GA) which transforms simple finite character strings into relatively complicated computer programs. In GP, the individual structure has flexible expression abilities such as symbol description, regulation and arithmetic expressions. Accordingly, GP has a broad range of engineering applications, especially in machine learning and molecular biology.

Inspired by biological gene expression, Ferreira integrated the benefits of GA and GP, and put forward a novel heuristic algorithm named gene expression programming (GEP) [24]. On one hand, GEP inherits the fixed-length linear coding in GA, which is simple and fast. On the other hand, GEP inherits flexible and variable tree structure in GP and utilises simple symbols to solve the loading problem. Compared with traditional evolutionary algorithms, GEP can significantly improve the accuracy of solution.

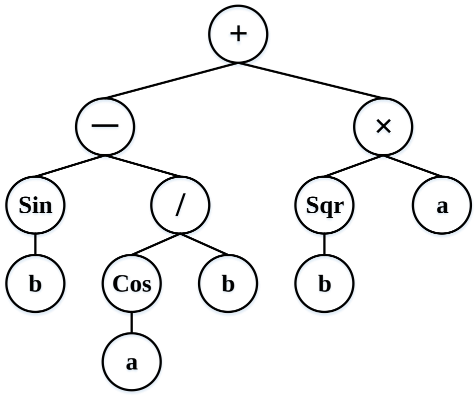

Fig. 5. Tree representation

The major superiority of GEP over GA/GP is unique individual coding method, which is able to overcome the shortcomings in GA and GP. In GEP, each gene consists of a tail and a head, where the tail includes the symbols from terminal set and the head includes the symbols from both function and terminal sets. The function set generally consists of mathematic operators such as '+', '–', '×', '⁄' while the terminal set consists of input variables and constants. Several similar genes with the same length form the GEP chromosome via a certain combination, which may be either logical operation or arithmetic operation, depending on real situation. Then, the chromosome is transformed into the configuration of expression tree (ET), which reads the gene from left to right and forms the ET in the hierarchical order. Fig. 5 shows an example of the tree structure of gene expression, in which ‘Sin’, ‘Cos’ and ‘Sqr’ denote Sine, Cosine and Squared operations. In tree configuration, the length of gene expression is 12 characters and the non-encoded area at the back of the gene provides the convenience for the program evolution.

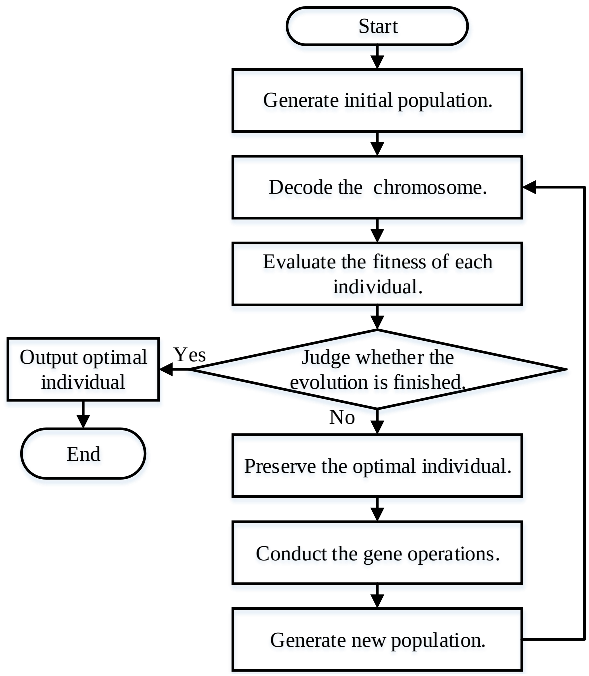

Fig. 6. Flowchart of GEP algorithm

Several genes with same length form the chromosome of the GEP via a certain combination, which can be either logic operation or arithmetic operation. When the program of the GEP is in operation, the gene number and gene head length are chosen beforehand. Each gene fragment in the chromosome could be decoded into a sub-expression tree. Multiple sub-expression trees can form a more complicated multi-subunit expression tree. This special configuration of GEP chromosome and abundant gene operators are capable of providing basic guarantee for the GEP to solve complex problems. Generally, the procedure of standard GEP includes the following steps [25], the flowchart of which is shown in Fig. 6.

Step 1. Set the control parameters, select the function sets and terminator.

Step 2. Build up initial population.

Step 3. Decode the gene code of GEP.

Step 4. Calculate each individual fitness value and evaluate whole population.

Step 5. Judge whether the algorithm reaches the maximum iteration number and pre-set calculation accuracy. If it is satisfied, the evolution process terminates and the optimal individual is obtained. Otherwise, go to Step 6.

Step 6. Implement optimal preservation strategy.

Step 7. Conduct the selection, replication, crossover, mutation and recombination operations to generate new population.

Step 8. Evaluate each individual fitness in new population, and subsequently go back to Step 5.

3. Data collection and description for model development

3.1. Factors related to elastic modulus of ASR-affected concrete

As all we know, ASR is a chemical reaction between alkalis in the concrete pore solution and some mineral phases (generally amorphous of poorly crystallized silica) from the aggregates used in concrete; the latter indicates that reactive aggregate and alkali content are the main sources for ASR generation. ASR is also dependent of the aggregate type (fine or coarse) and nature (i.e. lithotype). In addition, previous studies have shown that the elastic modulus has strong correlation to the compressive strength of concrete mixtures, which should be included as inputs for the development of the predictive model [14]. Moreover, the exposure condition of concrete such as high moisture and temperature may also affect ASR-induced expansion and damage. Based on these facts, 12 influential factors are considered as input variables for the prediction model, including content of cement (CC), ratio of water to cement (WCR), ratio of fine reactive aggregate to cement (FRACR), ratio of coarse reactive aggregate to cement (CRACR), ratio of non-reactive aggregate to cement (NRACR), relative humidity (RH), exposure temperature (ET), total initial concrete alkali content (AC), compressive strength (CS), curing time (CT), maximum potential expansion (MPE), and measured expansion (ME). The maximum potential expansion represents for the reactivity of aggregate used in the concrete mixtures.

3.2. Data collection

In this study, SC-based models will be developed to characterize highly nonlinear relationships between the aforementioned factors and elastic modulus degradation of concrete affected by ASR. However, to build up a reliable and robust model with high accuracy, it is of great necessity to obtain vast collection of data. Via extensive literature summary, over 200 groups of data were collected from 15 studies that were published between 1989 and 2017 [4-6, 15, 29-39]. In order to make sure the reliability of the data, several samples were excluded from the data set due to special curing conditions and or laboratory testing procedures. Eventually, 178 groups of data made up the data set used for developing SC models in this work, including 12 influence factors as presented and elastic modulus. All these data were measured from the specimens tested under free expansion conditions. Tests for determining the elastic modulus and compressive strength were conducted on cylindrical specimens with the size of 100×200 mm. The expansion values were measured on the same cylindrical specimens or on prism specimens in accordance with test standards. In this research, the elastic modulus degradation of concrete induced by ASR is expressed by the ratio of elastic modulus value of damaged concrete to corresponding value of sound specimen, shown in Eq. (23):

$$N_{Ec} = \frac{E_c^d}{E_c^u} \tag{23}$$

where E_c^u and E_c^d denote the elastic modulus of intact and ASR damaged concretes, respectively. According to the reference [4] in which the "damage" (i.e. mechanical properties degradation, cracking) of various reactive concrete mixture is tested at various expansion level, the damage is negligible at the expansion levels of less than 0.03%. In the studies where the data was collected, the elastic modulus of sound specimens were obtained at 7, 14 or 28 days of curing period when the expansion induced by ASR is at a relatively low level of less than 0.03%. Table 1 gives the statistical information of collected experimental data. It is obvious that most of these parameters are in the wide ranges except the relative humidity, the value of which is between 95% and 100%. Apparently, all the test specimens were stored under the condition of high moisture, so the collected information of relative humidity plays a negligible role in setting up the predicative model, and should be excluded from the model development. Accordingly, based on above analysis, the inputs of the SC models to be designed include CC, WCR, FRACR, CRACR, NRACR, ET, AC, CS, CT, MPE and ME, while the outputs of models are N_{Ec}.

Table 1 Statistical information of collected experimental data (Min: minimum, Max: maximum, SD: standard deviation, SEM: standard error of mean).

Parameters	Statistical index							
	Min	Max	Median	Average	SD	SEM	Skewness	Kurtosis
CC (kg/m^3)	300	424	370	367.4	44.107	3.306	-0.147	1.647
WCR	0.370	0.610	0.470	0.481	0.064	0.005	0.252	2.463
FRACR	0.000	2.850	0.000	0.995	1.130	0.085	0.359	1.307
CRACR	0.000	3.420	2.750	2.198	1.293	0.097	-1.016	2.258
NRACR	0.000	4.020	2.085	1.828	1.072	0.080	-0.647	2.398
ET (ºC)	38	50	38	39.7	3.756	0.282	2.290	6.520
RH (%)	95	100	100	98.5	2.033	0.508	-0.614	1.509
AC (%)	1.170	2.870	1.250	1.526	0.522	0.039	1.564	3.770
CS (MPa)	18.200	58.500	35.700	35.671	8.601	0.645	0.462	3.224
CT (day)	7	28	28	21.7	9.456	0.709	-0.870	1.796
MPE (%)	0.072	0.916	0.300	0.361	0.223	0.017	1.063	3.108
ME (%)	0.001	0.916	0.147	0.209	0.180	0.014	1.380	4.661
N_{Ec} (-)	0.163	1.130	0.628	0.624	0.230	0.017	-0.063	2.261

To guarantee the independency of each input variable, the correlation analysis is conducted on the model inputs and the correlation coefficient *R* between arbitrary two inputs is calculated using the following equation:

$$R_{i,j} = \frac{n_{to}\sum_{k=1}^{n_{to}} x_i(k)\cdot x_j(k)}{\sqrt{n_{to}\sum_{k=1}^{n_{to}} x_i(k)^2 - [\sum_{k=1}^{n_{to}} x_i(k)]^2}\cdot\sqrt{n_{to}\sum_{k=1}^{n_{to}} x_j(k)^2 - [\sum_{k=1}^{n_{to}} x_j(k)]^2} \tag{24}$$

where n_{to} denotes entire data sample number; x_i and x_j represent ith and jth inputs, respectively. Generally, the value of correlation coefficient should be between -1 and 1. If the absolute value of R between two input variables is above 0.8, it indicates the strong relationship between these two inputs and one input should be removed because it can be represented by a linear transformation of the other input. Table 2 shows the correlation analysis result of all the model inputs. It is noticeable that absolute values of all the correlation coefficients are below 0.7 except that of the diagonal line in the correlation coefficient matrix, where are self-correlation coefficients. Hence, all 11 input variables can be employed to design predictive models on basis of SC techniques.

Table 2 Correlation analysis result of input variables

Variable	CC	WCR	FRACR	CRACR	NRACR	ET	AC	CS	CT	MPE	ME
CC	1.000	-0.511	-0.107	-0.405	-0.013	-0.632	-0.592	0.466	0.276	-0.567	-0.341
WCR	-0.511	1.000	0.166	0.339	-0.029	0.403	0.493	-0.646	-0.213	0.372	0.237
FRACR	-0.107	0.166	1.000	-0.485	-0.369	-0.255	-0.039	-0.162	-0.364	-0.069	0.022
CRACR	-0.405	0.339	-0.485	1.000	-0.482	0.341	0.411	-0.140	-0.203	0.213	0.152
NRACR	-0.013	-0.029	-0.369	-0.482	1.000	0.239	-0.021	-0.083	0.470	0.160	0.002
ET	-0.632	0.403	-0.255	0.341	0.239	1.000	0.568	-0.336	-0.278	0.628	0.410
AC	-0.592	0.493	-0.039	0.411	-0.021	0.568	1.000	-0.548	-0.432	0.483	0.534
CS	0.466	-0.646	-0.162	-0.140	-0.083	-0.336	-0.548	1.000	0.254	-0.426	-0.348
CT	0.276	-0.213	-0.364	-0.203	0.470	-0.278	-0.432	0.254	1.000	-0.239	-0.177
MPE	-0.567	0.372	-0.069	0.213	0.160	0.628	0.483	-0.426	-0.239	1.000	0.622
ME	-0.341	0.237	0.022	0.152	0.002	0.410	0.534	-0.348	-0.177	0.622	1.000

4. Results and discussions

Five SC models are developed and evaluated based on the collected data samples, which are separated into two subsets randomly. First set with 125 groups of data (70%) is utilized to train five SC models while second set with 53 groups of data (30%) is utilized to test the capacities of trained models. Finally, the developed predictive models are appraised and compared to empirical models with regard to several statistical evaluation indices.

4.1. Results of SC techniques to predict elastic modulus of ASR-affected concrete

4.1.1. ANN results

The ANN is implemented using MATLAB V2015a neural network toolbox. A three-layer network structure, including an input layer, a hidden layer and an output layer, is employed to develop the ANN model for formulating elastic modulus degradation of concrete because of ASR. Before the model is trained, the neuron number in hidden layer and transfer functions in hidden and output layers should be determined beforehand. In this study, due to excellent nonlinear regression capacity, the log-sigmoid function is selected as transfer functions in both layers to nonlinearly transform the information from previous layers, the output of which is in the range of [0, 1]. The corresponding mathematical expression is given in Eq. (25):

$$LS(x) = -1 + \frac{2}{1+e^{-2x}} \tag{25}$$

Generally, determination of neuron number in hidden layer rests with the problem in practice. Previous studies have shown that the following empirical formula can be adopted to choose optimal hidden neuron number [40]:

$$m_h = \tau + \sqrt{m_{in} + m_{out}} \tag{26}$$

where m_{in}, m_h and m_{out} represent the input, hidden and output neuron numbers, respectively. τ denotes a constant between 1 and 10. Therefore, the optimal hidden neuron number m_h should be in a range. Since the inputs and output of ANN model are CC, WCR, CRACR, NRACR, ET, AC, CS, CT, MPE, ME and N_{Ec}, the range of hidden neuron number is [5, 13]. Then, trial-and-error method is utilized to find the best number of hidden neurons via minimizing mean square error (MSE) between predicted elastic modulus degradations from the ANN and corresponding real values in training samples. The expression of MSE is given as follows:

$$MSE = \frac{1}{N_{tr}} \sum_{k=1}^{N_{tr}} [N_{Ec}^{p}(k) - N_{Ec}^{r}(k)]^2 \tag{27}$$

where $N_{Ec}^{p}(k)$ and $N_{Ec}^{r}(k)$ denote predicted and real elastic modulus degradations in *k*th training sample, respectively.

Training an ANN model is generally regarded as the procedure of adjusting the values of connection weights and bias to get the optimal generalization ability using training algorithms. In this part, three commonly used training algorithms, namely Levenberg-Marquardt (LM) optimization, Bayesian regularization (BR) and conjugate gradient back-propagation with Powell-Beale restarts (CGP), are employed to train the model to find hidden neuron number with optimal network performance. Fig. 7 displays the MSEs of ANN models corresponding to different training algorithms and hidden neuron numbers. It is clearly seen that compared with LM and CGP, BRP training algorithm has the lowest MSEs of ANN models with all possible hidden neuron numbers. The major reason for this result is that BR neural network is much more robust than general back-propagation networks, and is able to eliminate or decrease the requirement for redundant validation existing in LM and CGP training algorithms. Hence, the BR algorithm is selected as training algorithm to optimize the network parameters. For the hidden neuron number, it is obvious that the MSE of model declines initially with the increase of number, and keep stable after the hidden neuron number arrives at 8, corresponding to the MSE of 0.0015. To simplify the network configuration, the neuron number in the hidden layer is set as 8 accordingly.

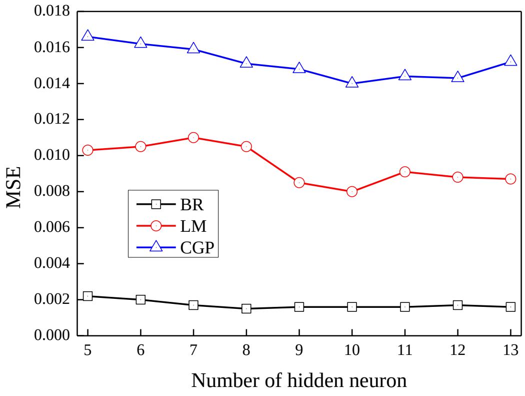

Fig. 7. MSEs of the ANN models with different numbers of hidden neuron

Afterwards, the testing data are applied to trained ANN model to evaluate its performance. Fig. 8 shows the comparisons between predictions from ANN model and corresponding measured elastic modulus degradations of ASR-affected concrete for both training and testing samples. MSE and correlation coefficient are adopted as evaluation indices to assess the effectiveness of developed ANN model. It is clearly seen that most data points are dispersed on both sides of regression line uniformly, which indicates perfect matching between measured results and model predictions. The correlation coefficients for both training and testing cases are 0.9841 and 0.9261, meeting the requirement of relevance. Consequently, the developed ANN model exhibits good capacity to characterize elastic modulus degradation of concrete due to ASR.

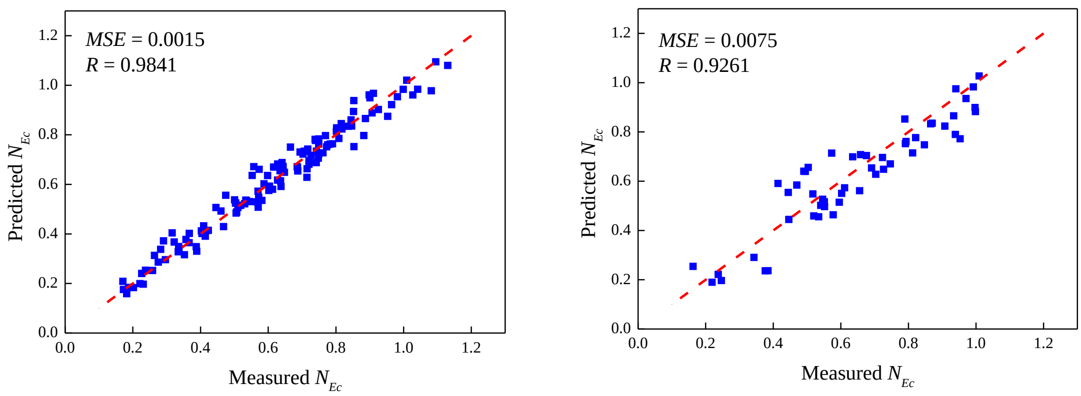

(a) (b)

Fig. 8. Comparisons between real elastic modulus degradations and the results predicted from the ANN model, (a) training; (b) testing.

4.1.2. SVM results

The SVM model is implemented using MATLAB V2015b LibSVM toolbox. To guarantee high accuracy of the developed predictive model, the hyper-parameters in the SVM should be assigned with reasonable values [41]. Here, the hyper-parameters include penalty parameter C, kernel function parameter σ and insensitive loss factor ε, which have been introduced in Section 2.2. Different parameter combinations may cause notably distinct generalization capacities of the developed model. Therefore, it is of definite necessity to obtain the best parameter combination for developing SVM model, which is usually deemed as solving a minimum optimization problem. To avoid the over-fitting of the trained SVM model, in this study the optimization target is defined as MSE of 5-fold cross-validation and the expression is shown in Eq. (28):

$$MSE_{cv} = \frac{1}{5}\sum_{k=1}^{5}\sum_{j=1}^{N_{cv}}[N_{Ec}^{p}(k,j) - N_{Ec}^{r}(k,j)]^2 \tag{28}$$

According to Eq. (28), the training data is randomly divided into 5 groups. For each time, *k*th (*k*=1, 2, …, 5) group of data is used as the validation data while the rest is used as the samples to train the SVM. Finally, the mean value of MSE of 5 groups of validation data is the optimization target for its minimum value. The procedure of SVM parameter optimization using particle swarm optimization (PSO) algorithm is composed of following five steps:

Step 1. Set PSO parameters, such as population number, inertia weight, two learning coefficients, maximum iteration number and scales of location and velocity. In this study, the population number is set as 30, inertia weight is set as 0.6, two learning coefficients are set as 1.5 and 1.7, maximum iteration number is set as 200, lower limit of location is set as [0.1 0.01 0.001], upper limit of location is set as [100 1000 100], lower limit of velocity is set as [0 0 0], and upper limit of velocity is set as [2 2 2].

Step 2. Assign initial values of location and velocity of each particle randomly.

Step 3. Based on the training samples, evaluate the fitness (target) value of each particle.

Step 4. Compare the current individual and global optima to the records. If the current optima are better than previous ones, replace the records with current solutions. Otherwise, keep the individual and global optima unchanged.

Step 5. Use Eq. (29) and Eq. (30) to update the velocities and locations of particles in the swarm.

$$v_k^{j+1} = w \cdot v_k^j + lc_1 \cdot c_1 \cdot (ib_k^j - x_k^j) + lc_2 \cdot c_2 \cdot (sb^j - x_k^j) \tag{29}$$

$$x_k^{j+1} = x_k^j + v_k^{j+1} \tag{30}$$

where w is inertia weight, lc_1 and lc_2 are two learning factors, c_1 and c_2 denote two random values between 0 and 1.

Step 6. Evaluate the algorithm termination. If current iteration number exceeds the maximum iteration number, the algorithm terminates. Otherwise, go back to Step 3.

Fig. 9 describes the changing processes of fitness and three parameters when the PSO is used to optimize the SVM model for predicting elastic modulus of concrete affected by ASR. It is noticeable that optimal fitness value reduces with the increase of iteration number and becomes stable after around 90 iterations, even though the mean fitness fluctuates from the beginning to the end. Moreover, different parameters exhibit diverse variation tendencies during the algorithm iteration. Apparently, parameters C and σ fluctuate in the early stage of evolution and then stabilize while parameter ε remains unchanged in the iteration process. After the SVM model is built up, the testing data is used to assess its capacity for elastic modulus prediction. Fig. 10 displays the comparisons between experimental values and SVM predictions for both training and testing data. Similar to ANN model, the SVM model demonstrates high accuracy in predicting elastic modulus degradation, with the MSEs of 0.0019 and 0.0031 and the values of correlation coefficient of 0.9827 and 0.9404.

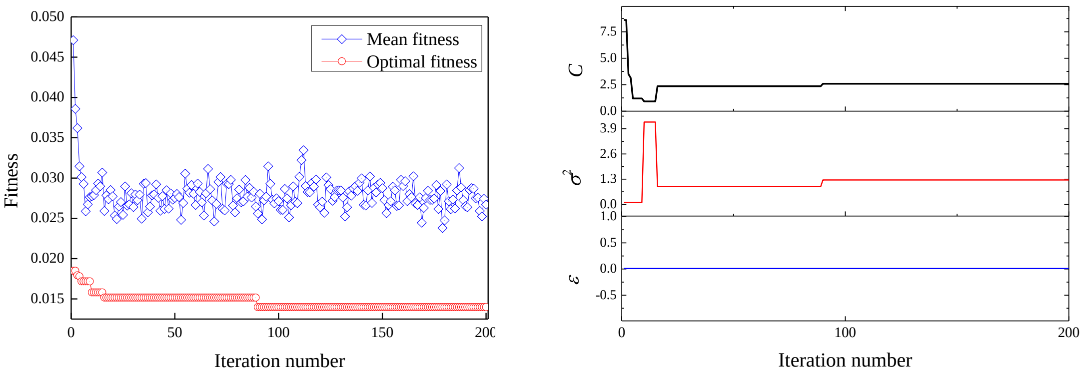

(a) (b)

Fig. 9. SVM model optimization, (a) fitness variation; (b) parameter variation.

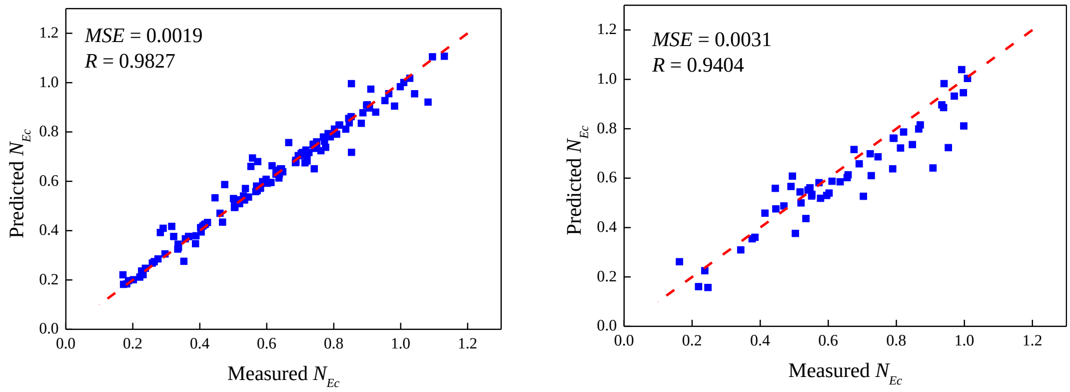

(a) (b)

Fig. 10. Comparisons between real elastic modulus degradations and the results predicted from the SVM model, (a) training; (b) testing.

4.1.3. ANFIS results

To develop a reliable and robust ANFIS, several important model parameters should be properly assigned in advance, including type and number of membership function as well as epoch number. Generally, the membership function is used to demonstrate antecedent part of ANFIS, which can be deemed as linguistic variable. In order to decrease the model complexity, five membership functions are selected in this study, which correspond to linguistic variables of very small, small, medium, big and very big. Furthermore, the Gaussian function is used as the membership function due to perfect nonlinear prediction capacity. Based on the training data, the fuzzy inference system is generated by fuzzy c-means clustering method, which can extract a group of fuzzy rules to characterize highly nonlinear relationship between model inputs and output. Fig. 11 portrays the membership function of each input variable and corresponding linguistic variable. It is noticeable that the shapes of several membership functions of input variables change from initial stage to final stage, such as WCR, AC, MPE and ME. Fig. 12 (a) gives the comparison between real elastic modulus values and ANFIS prediction for training data. Compared to SVM and ANN models, the ANFIS has higher correlation coefficient (0.9934) and lower MSE (0.0007) in training.

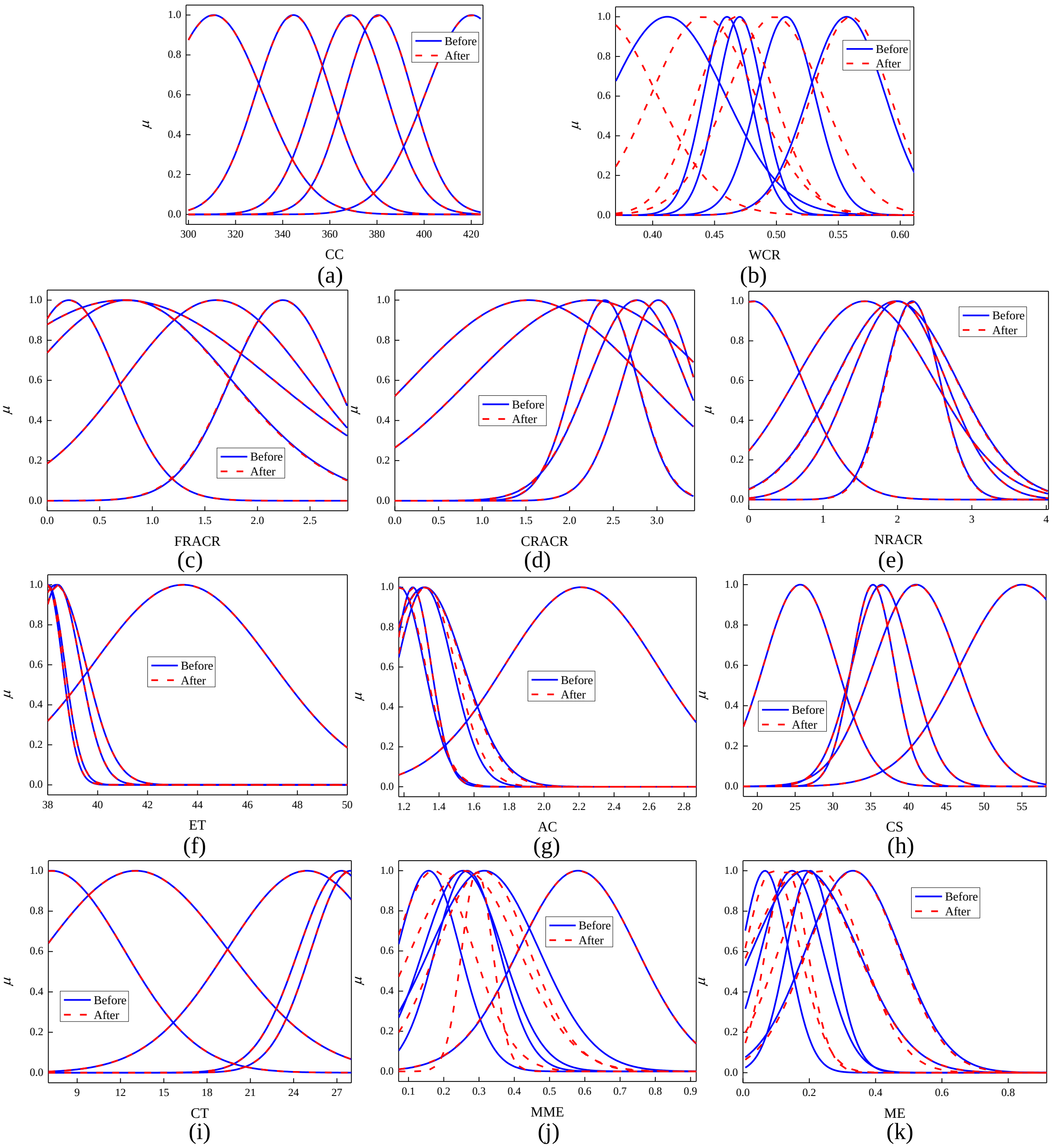

Fig. 11. Membership functions of input variables before and after model training, (a) CC; (b) WCR; (c) FRACR; (d) CRACR; (e) NRACR; (f) ET; (g) AC; (h) CS; (i) CT; (j) MPE; (k) ME.

Then, the testing data is sent to the developed ANFIS for prediction capacity evaluation and the result is shown in Fig. 12 (b). Even though the value of correlation coefficient (0.9078) of ANFIS model is worse than that of SVM and ANN models for testing samples, it is still good enough as the forecast tool for elastic modulus deterioration since the MSE value is 0.0038 which is main target of model performance.

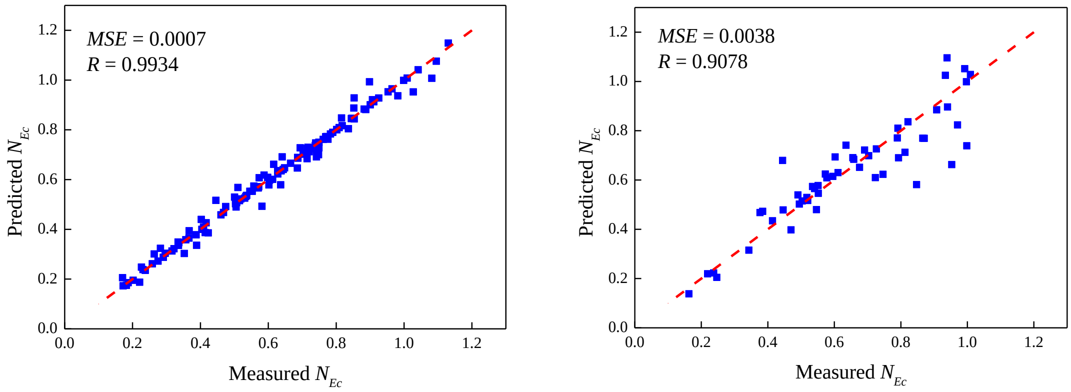

(a) (b)

Fig. 12. Comparisons between real elastic modulus degradations and the results predicted from the ANFIS model, (a) training; (b) testing.

4.1.4. M5P results

In this part, all the parameters that can affect the concrete elastic modulus reduction due to ASR are employed to develop the M5P model and a linear multi-variable regression formula is selected with the following expression:

$$M = a_0 + a_1\text{x}1 + a_2\text{x}2 + a_3\text{x}3 + a_4\text{x}4 + a_5\text{x}5 + a_6\text{x}6 + a_7\text{x}7 + a_8\text{x}8 + a_9\text{x}9 + a_{10}\text{x}10 + a_{11}\text{x}11 \quad (31)$$

where M denotes the normalized elastic modulus N_{Ec}, and xi (i=1,…,11) denote CC, WCR, FRACR, CRACR, NRACR, ET, AC, CS, CT, MPE and ME, respectively. Based on Eq. (31), the model trees are established and shown in Fig. 13. It is clearly seen that these model trees provide the assessment of elastic modulus deterioration caused by ASR. The term 'M' at tree leave represents the linear sub-model identified by the M5P model. Table 3 gives the corresponding values of coefficients in Eq. (31) for each sub-model tree.

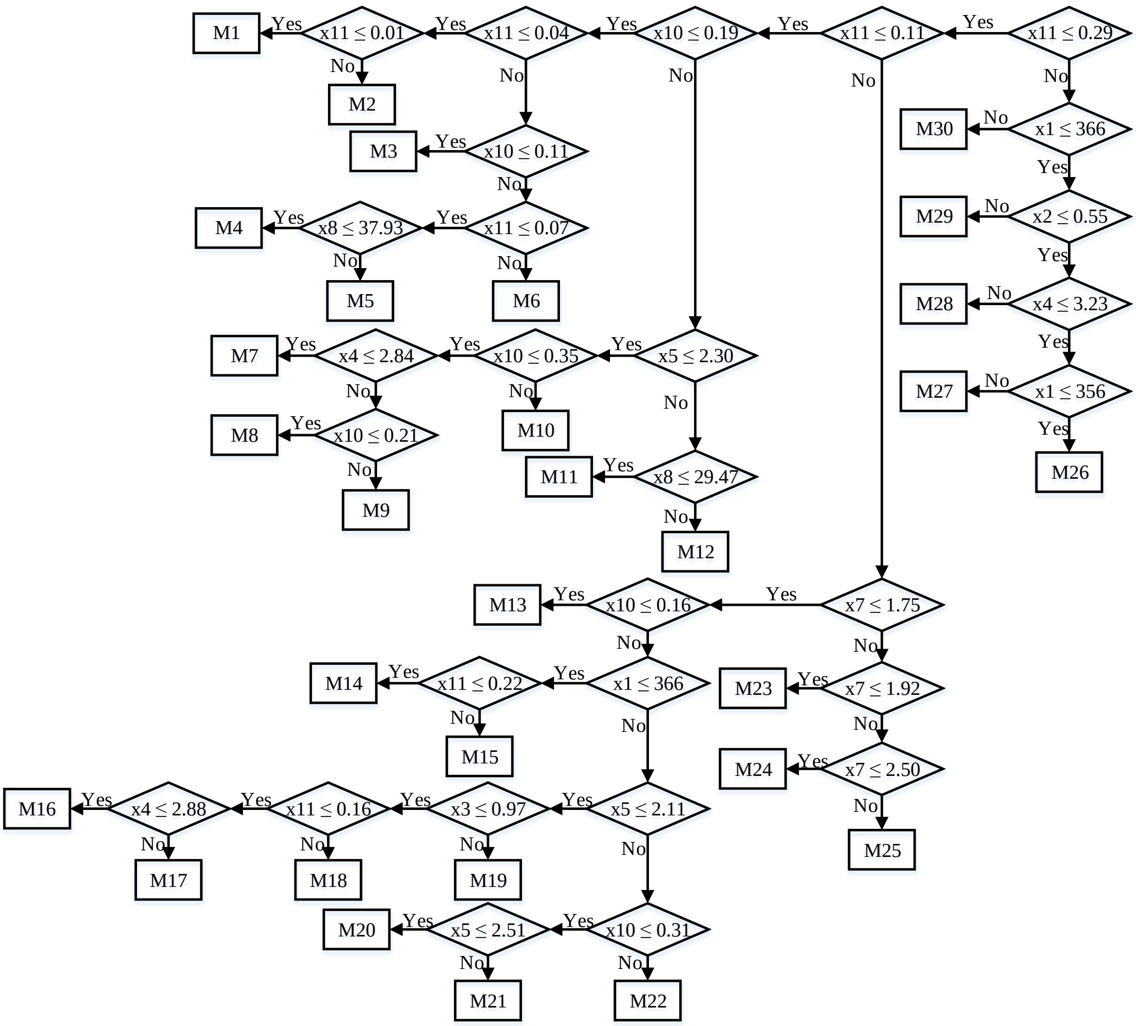

Fig. 13. Generated model tree structure of M5P for predicting elastic modulus reduction

Table 3 Expressions and codes of sub-model trees

Model expression	Code of model tree		
M1 = 1.0457	if x11 ≤ 0.29	else	if x10 ≤ 0.31
M2 = 1.1415 -0.0044·x8	if x11 ≤ 0.11	if x8 ≤ 29.47	if x5 ≤ 2.51
M3 = 0.9334	if x10 ≤ 0.19	y = 0.5859	y = 0.5479
M4 = 0.8493	if x11 ≤ 0.04	else	else
M5 = 0.8269	if x11 ≤ 0.01	y = 0.7092	y = 0.4327
M6 = 0.8004	y = 1.0457	else	else
M7 = 0.7405	else	if x7 ≤ 1.75	y = 0.7566 -0.8371·x11
M8 = 0.7544	y = 1.1415 -0.0044·x8	if x10 ≤ 0.16	else
M9 = 0.8212	else	y = 0.7674	if x7 ≤ 1.9188
M10 = 0.9361	if x10 ≤ 0.11	else	y = 1.1128
M11 = 0.5859	y = 0.9334	if x1 ≤ 366	else
M12 = 0.7092	else	if x11 ≤ 0.22	if x7 ≤ 2.5036
M13 = 0.7674	if x11 ≤ 0.07	y = 0.4871	y = 0.7838
M14 = 0.4871	if x8 ≤ 37.93	else	else
M15 = 0.3064	y = 0.8493	y = 0.3064	y = 0.4898
M16 = 0.5501 +1.4702·x11	else	else	else
M17 = 0.6211	y = 0.8269	if x5 ≤ 2.11	if x1 ≤ 366
M18 = 0.3463 +1.3711·x10	else	if x3 ≤ 0.97	if x2 ≤ 0.55
M19 = 2.4843 -0.0051·x1	y = 0.8004	if x11 ≤ 0.16	if x4 ≤ 3.23
M20 = 0.5479	else	if x4 ≤ 2.88	if x1 ≤ 356
M21 = 0.4327	if x5 ≤ 2.30	y = 0.5501	y = 0.3157
M22 = 0.7566 -0.8371·x11	if x10 ≤ 0.35	+1.4702·x11	else
M23 = 1.1128	if x4 ≤ 2.84	else	y = 0.2429

M24 = 0.7838 M25 = 0.4898 M26 = 0.3157 M27 = 0.2429 M28 = 0.2020 M29 = 0.3512 -1.0298·x10 +1.0936·x11 M30 = 0.6437 -0.0802·x3	y = 0.7405 else if x10 ≤ 0.21 y = 0.7544 else y = 0.8212 else y = 0.9361	y = 0.6211 else y = 0.3463 +1.3711·x10 else y = 2.4843 -0.0051·x1 else	else y = 0.2020 else y = 0.3512 -1.0298·x10 +1.0936·x11 else y = 0.6437 -0.0802·x3

Fig. 14 displays the comparisons between experimental results and results from M5P model for both training and validation data. Similar to ANN, SVM and ANFIS models, M5P model has higher correlation coefficient (R) and lower MSE for training data, i.e. 0.9835 and 0.0018. The R and MSE of M5P model using validation data, however, are not as good as that of SVM and ANN. Overall, the R of 0.9023 and MSE of 0.0051 are acceptable in modeling study and the developed M5P model could be utilized as a selection for predicting ASR induced elastic modulus degradation accordingly.

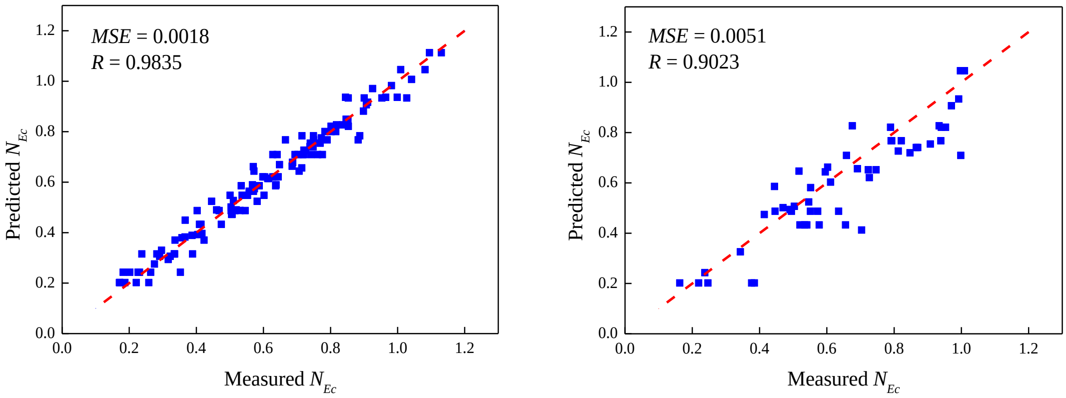

(a) (b)

Fig. 14. Comparisons between real elastic modulus degradations and the results predicted from the M5P model, (a) training; (b) testing.

4.1.5. GEP results

In this study, the GEP model is designed using GeneXproTools 5.0 and the final program is transformed into MATLAB code for practical implementation. The mathematical operators and functions used to develop the GEP for predicting the elastic modulus reduction caused by ASR include '–', '+', '⁄', '×', Exp, Avg, Inv, Min, Max, Atan, Tanh and Not, where Exp denotes the exponential function, Avg denotes average operation, Inv denotes inverse operation, Min and Max respectively indicate the minimization and maximization operations, Atan denotes the arctangent function, Tanh denotes hyperbolic tangent function, and Not denotes the function that 1 subtracts the variable. The parameters of the GEP are set according to the trial runs that can ensure the robustness and generalization of the developed model. Generally, the chromosome number determines the running time of the program. A larger chromosome number may contribute to the GEP model with lower error but can cause longer running time. The appropriate number of chromosome in practice is dependent on the model complexity and potential solution number. Besides, the gene number and size of head, advancing the chromosome features in the model, elaborate the sub-ET number and gene complexity, respectively. A larger gene number can lead to a complicated function with over-fitting problem. To obtain the optimal parameter values of GEP, the trial-and-error strategy is selected via five different running of the program. Finally, the parameter setting of GEP is shown in Table 1. Furthermore, a fitness function is required for the GEP development. In this study, similar to that in other SC models, the MSE between experimental values and model outputs as fitness function.

Table 4 Setting of GEP parameters

Parameter	Settings
General	
Chromosome number	300
Size of head	4
Number of genes	20
Linking function	Multiplication
Genetic operator	
Inversion rate	0.15
Mutation rate	0.05
One point recombination rate	0.4
Two points recombination rate	0.4
Gene transposition rate	0.15
Gene recombination rate	0.15
IS Transportation rate	0.2
RIS transportation rate	0.2
Numerical constants	
Constants per gene	10
Lower bound	-10
Upper bound	10
Data type	Floating-point
Complexity increase	
Generations without change	2000
Maximum complexity	6
Trial number	3

Then, training and testing samples are adopted to develop and test GEP model in terms of elastic modulus reduction evaluation, respectively. Fig. 15 shows the modeling result, i.e. architectures of sub expression trees, the corresponding equations of which are given as follows.

$$N_{Ec} = outET1 \cdot outET2 \cdot outET3 \cdot outET4 \cdot outET5 \cdot outET6 \tag{32}$$

$$outET1 = \frac{1}{\frac{(ME \cdot 2) \cdot (CT + NRACR) + (CT + 1.5726)}{2} \cdot \left(9.7628 + e^{ME}\right)} \tag{33}$$

$$outET2 = (\mathrm{atan}(CRACR - FRACR + 6.7806)) \cdot \frac{-\frac{ET}{3.8433} + (\min(WCR, CS) - 5.0424)}{2} \tag{34}$$

$$outET3 = \frac{(AC \cdot 2) + 58.1214}{2} - \left(1 - (AC + 5.9572)\right) + \frac{1.4228}{\min(CT, MME)} \tag{35}$$

$$outET4 = \frac{1}{\left(\frac{CRACR - ET \cdot 8.1852 + CRACR}{2}\right) + \left(\frac{WCR + \tanh(NRACR)}{2}\right)} \tag{36}$$

$$outET5 = 1 - (\min(NRACR, CC) - (\max((NRACR - 1.3552), \frac{MME + AC}{2}) + \operatorname{atan}(ET) + CT)) \tag{37}$$

$$outET6 = \operatorname{atan}((\frac{-4.4089 \cdot (-4.4089 - CT) + (FRACR - CT)}{2}) - \frac{AC}{0.5418} \cdot \max(4.0822, MME)) \tag{38}$$

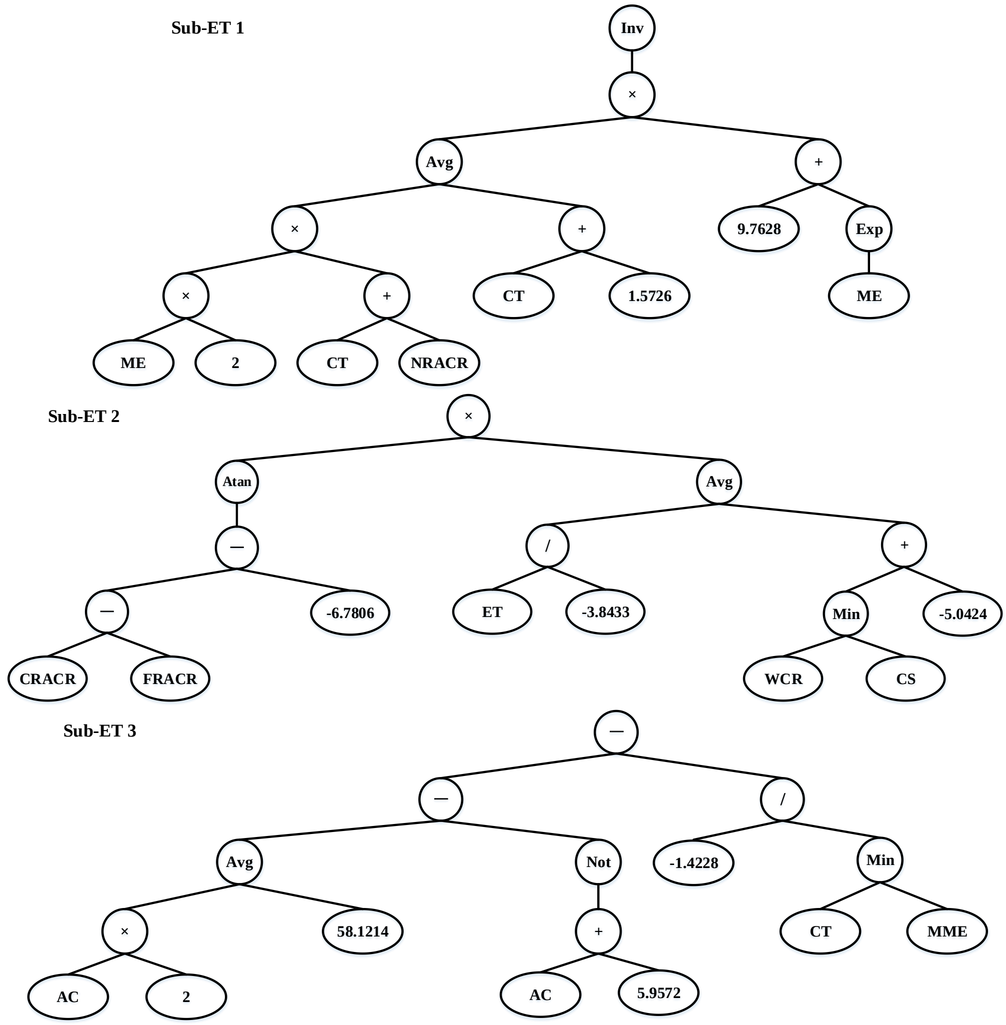

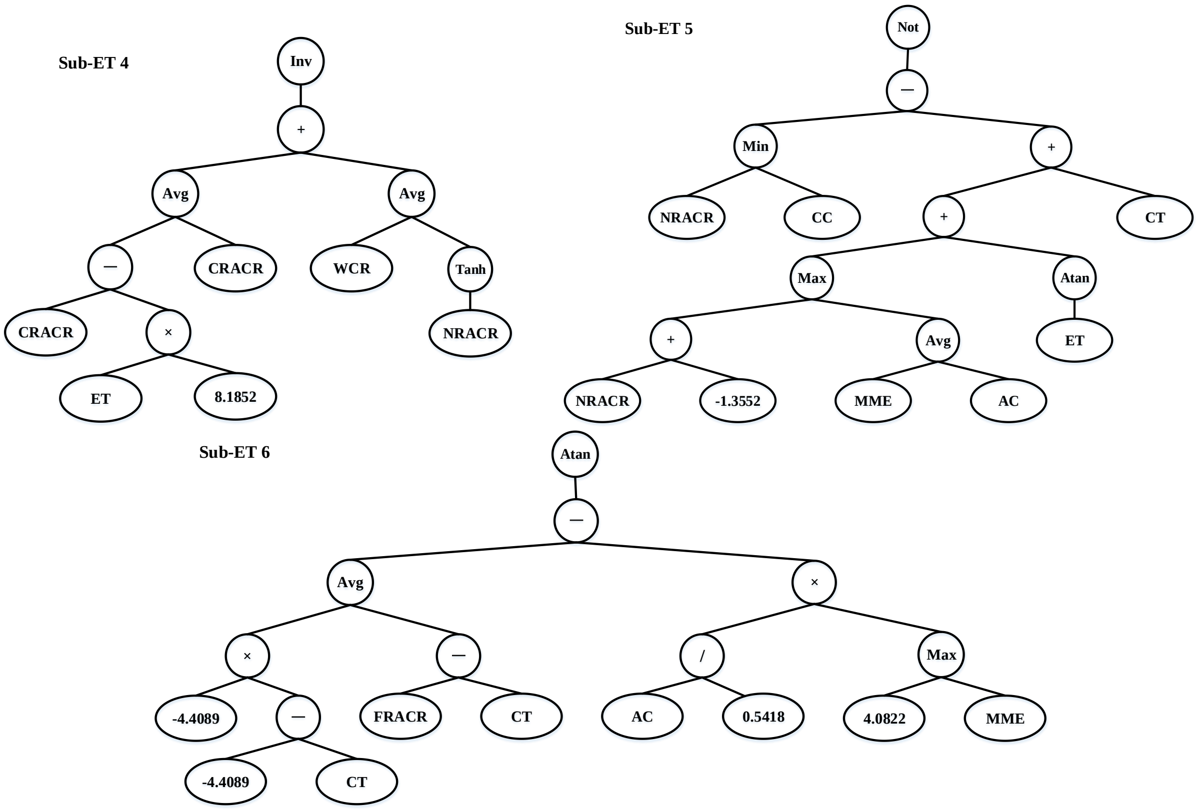

Fig. 15. Expression tree for predicting elastic modulus reduction

Fig. 16 gives the comparison between measured results and the predictions from GEP for training and testing data. According to the results in figures, it is noticeable that the values of MSE and R for the training data are worse than that for the testing data. Even though correlation coefficient value for training data is below 0.9, the corresponding value for testing data is 0.9061, which is even higher than that of M5P model. Consequently, the developed GEP model is able to be still regarded as an effective candidate for the elastic modulus deterioration prediction of ASR-affected concrete.

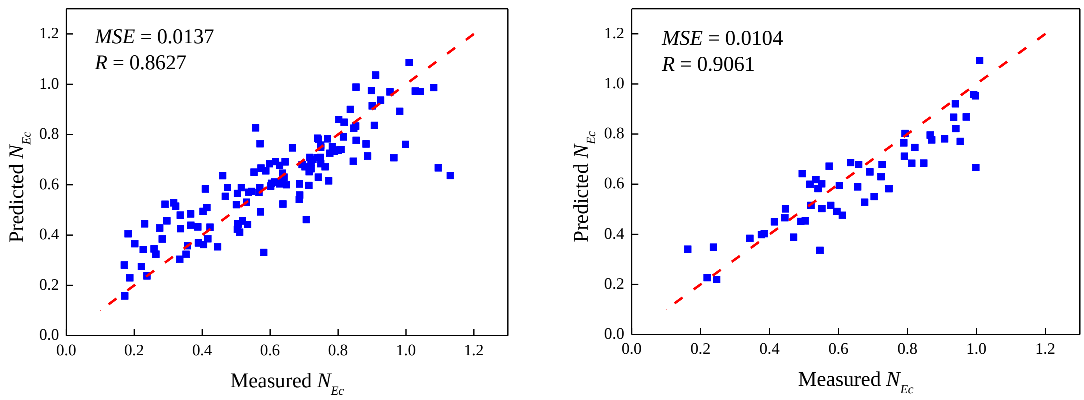

(a) (b)

Fig. 16. Comparisons between real elastic modulus degradations and the results predicted from the GEP model, (a) training; (b) testing.

4.2. Comparison with existing empirical models

To further illustrate the superiorities of developed SC methods, a comparative investigation is carried out in this part via the performance comparison between SC-based models and empirical models. These empirical models were developed by different researchers to relate the degradation of concrete elastic modulus caused by ASR to the expansion level. Table 5 provides the detailed information of these models, in which β_0, β_∞, ε_1, ε_c, p_l, q_l, q_m, q_h, q_e, d_{max}, ω and ε_0, are parameters to be identified based on experimental results. Obviously, in these models, the normalized elastic modulus is the function of the expansion level ε caused by ASR. In this study, to make a fair comparison, the same training and validation samples are employed to set up and test empirical models, which indicates that the optimal model parameters are identified using training samples and model performances are evaluated using testing samples. Here, the least square approach is adopted to estimate optimal values of parameters in three empirical models via curve fitting, and the identification results are shown in Table 6.

Table 5 Empirical models for predicting elastic modulus of ASR-affected concrete

Model index	Expression	Reference
Empirical model 1 (EM1)	$\beta_P = \frac{P}{P_{ref}} = \beta_0 - (\beta_0 - \beta_\infty) \cdot \frac{1-e^{-\frac{\varepsilon}{\varepsilon_c}}}{1+e^{-\frac{\varepsilon-\varepsilon_1}{\varepsilon_c}}}$ (39)	Saouma and Perotti (2006) [26]
Empirical model 2 (EM2)	$N_{E_c} = \frac{E_c}{E_c^r} = \begin{cases} p_l + q_l \cdot \varepsilon \\ p_m + q_m \cdot \varepsilon \\ p_h + q_h \cdot \varepsilon \\ p_e + q_e \cdot \varepsilon \end{cases}$ (40) $p_m = 0.05 \cdot (q_l - q_m) + p_l$ (41) $p_h = 0.1 \cdot (q_m - q_h) + p_m$ (42) $p_e = 0.5 \cdot (q_h - q_e) + p_h$ (43)	Esposito et al. (2016) [15]
Empirical model 3 (EM3)	$E_c = E_{c0} \cdot (1-d)$ (44) $d = d_{max} \cdot [1 - \exp(-\omega \cdot \langle \varepsilon - \varepsilon_0 \rangle^+)]$ (45)	Seignol et al. (2009) [27], Kawabata et al. (2017) [42], Martin et al. (2017) [43]

Table 6 Optimal parameter values of empirical models

Parameter	Value
β_0	0.9228
β_∞	0.1881
ε_1	0.0031
ε_c	-5.6370
p_l	1.0311
q_l	-5.0082
q_m	-1.5030
q_m	-1.0651
q_e,	-0.0472
d_{max}	0.7362
ω	456.5000
ε_0	0

Then, the testing samples are inputted into the empirical models with optimal parameters for evaluating model prediction capacities of elastic modulus degradation caused by ASR. Figs 17-19 depict the comparisons between real values and the predictions from three empirical models. It is noted that the MSE values of empirical models are around 0.02 for training samples and 0.007 for testing samples while the CC values are in the ranges of [0.78, 0.79] for training samples and [0.81, 0.82] for testing samples, which are much worse than the corresponding indices of SC models. The main reason for this phenomenon is that empirical models just consider the expansion level as the influence factor to predict the mechanical property, while in the SC-based models, other factors which directly influence the elastic modulus of concrete affected by ASR are also considered in addition to the expansion level.

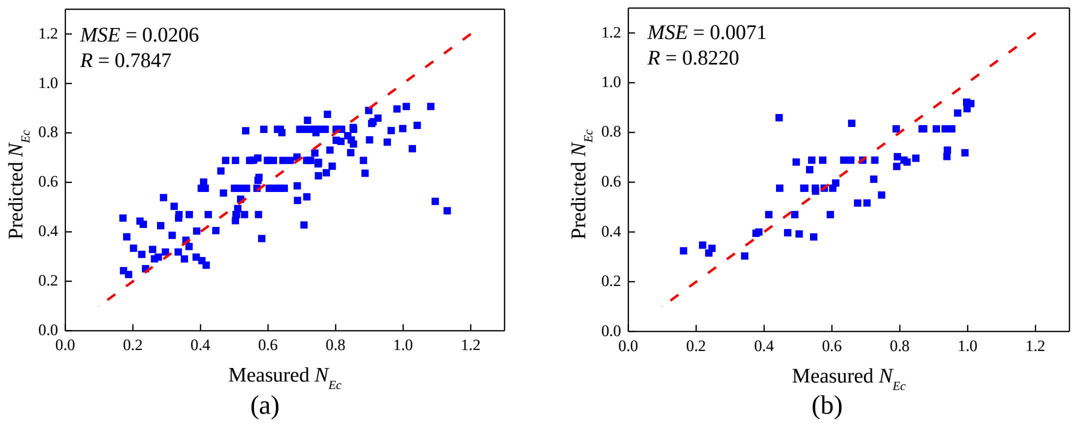

Fig. 17. Comparisons between real elastic modulus degradations and the results predicted from the empirical model EM1, (a) training; (b) testing.

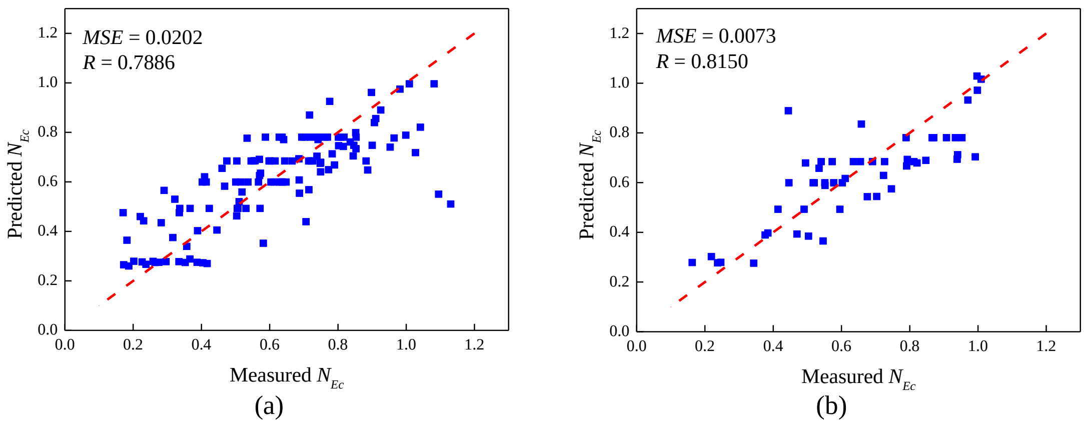

Fig. 18. Comparisons between real elastic modulus degradations and the results predicted from the empirical model EM2, (a) training; (b) testing.

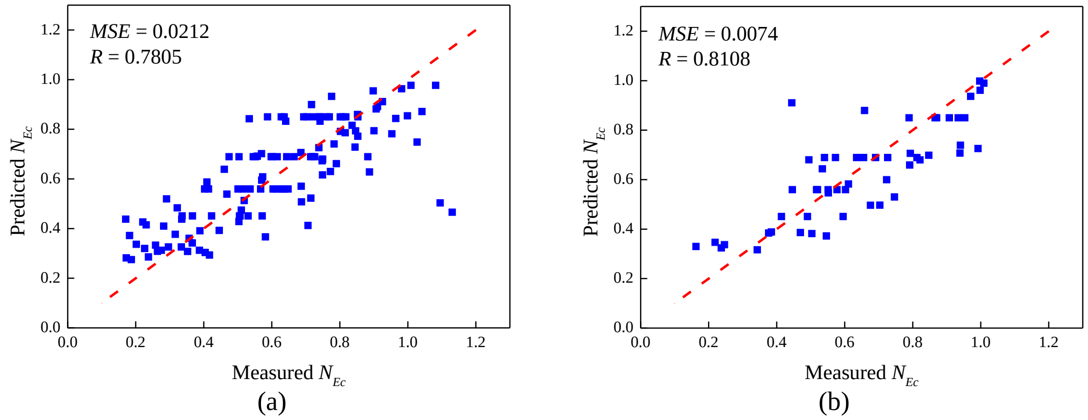

Fig. 19. Comparisons between real elastic modulus degradations and the results predicted from the empirical model EM3, (a) training; (b) testing.

Fig. 20 depicts the box-plot for the relative error distributions between experimental elastic modulus reductions and the outputs of all the models for all the data samples. It is noticeable that the median values of relative errors are close to 0 for all the eight predictive models. Compared with ANN, SVM, ANFIS and M5P, the GEP and three empirical models have wider ranges of relative error, which indicates the lower prediction accuracies. ANFIS has the best prediction performance for all the data samples, which can be reflected in the shortest distance between upper and lower error boundaries. It could be illustrated by excellent prediction results of training data, the MSE of which is only 0.0007. However, the range of the outliers of the ANFIS is wider than that of SVM, ANN and M5P models. On the whole, the proposed SC models outperform three empirical models in terms of relative error of elastic modulus prediction for all the data.

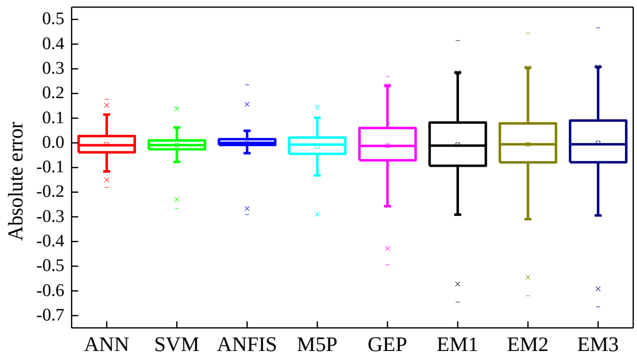

Fig. 20. Absolute error distributions of eight models for forecasting elastic modulus of ASR-affected concrete

Further, to comprehensively evaluate developed SC models with empirical models, more statistical evaluation indices are considered for performance comparison, including mean absolute error (MAE), mean absolute percentage error (MAPE), mean forecast error (MFE), error to signal ratio (ESR) and relative root mean square error (RRMSE). Corresponding mathematical equations of five evaluation indices are provided as follows.

$$MAE = \frac{1}{N_{to}} \sum_{k=1}^{N_{to}} \left| N_{Ec}^{p}(k) - N_{Ec}^{r}(k) \right| \quad (46)$$

$$MAPE = \frac{100}{N_{to}} \sum_{k=1}^{N_{to}} \left| \frac{N_{Ec}^{p}(k) - N_{Ec}^{r}(k)}{N_{Ec}^{r}(k)} \right| \quad (47)$$

$$MFE = \frac{1}{N_{to}} \sum_{k=1}^{N_{to}} [N_{Ec}^{p}(k) - N_{Ec}^{r}(k)] \quad (48)$$

$$ESR = \frac{\frac{1}{N_{to}} \sum_{k=1}^{N_{to}} [N_{Ec}^{p}(k) - N_{Ec}^{r}(k)]^2}{\frac{1}{N_{to}} \sum_{k=1}^{N_{to}} [N_{Ec}^{p}(k) - \frac{1}{N_{to}} \sum_{k=1}^{N_{to}} N_{Ec}^{p}(k)]^2} \quad (49)$$

$$RRMSE = \frac{100}{N_{to}} \sum_{k=1}^{N_{to}} [\frac{N_{Ec}^{p}(k) - N_{Ec}^{r}(k)}{N_{Ec}^{r}(k)}]^2 \quad (50)$$

The lower values of these indices indicate better performance of evaluated model. Fig. 21 describes the radar plot for evaluation indices of each predictive model for all the data samples. It is clearly observed that the ANFIS has the best performance among all the predictive models in terms of MAE, MAPE, ESR and RRMSE. The relative differences of MAE, MAPE, ESR and RRMSE between ANN and ANFIS models are 48%, 61%, 13% and 35%, respectively. The relative differences of MAE, MAPE, ESR and RRMSE between SVM and ANFIS models are 26%, 36%, 20% and 30%, respectively. The relative differences of MAE, MAPE, ESR and RRMSE between M5P and ANFIS models are 59%, 70%, 56% and 42%, respectively. The relative differences of MAE, MAPE, ESR and RRMSE between GEP and ANFIS models are 181%, 228%, 467% and 190%, respectively. The relative differences of MAE, MAPE, ESR and RRMSE between EM1 and ANFIS models are 254%, 304%, 882% and 246%, respectively. The relative differences of MAE, MAPE, ESR and RRMSE between EM2 and ANFIS models are 248%, 298%, 825% and 247%, respectively. The relative differences of MAE, MAPE, ESR and RRMSE between EM3 and ANFIS models are 251%, 307%, 757% and 247%, respectively. Apparently, from the indices of MAE, MAPE, ESR and RRMSE, the performances of GEP, EM1, EM2 and EM3 are worse than that of SVM, ANN, ANFIS and M5P models. Even though the MFE index of EM3 (0.0004) is better than that of ANFIS model (0.0031), this doesn’t imply that the EM3 has higher accuracy than the ANFIS model with regard to elastic modulus prediction of concrete affected by ASR. This is owing to the truth that except the unbiasedness of evaluated model, the MFE is unable to veritably reflect the deviation between real value and model prediction. Generally, only one evaluation index is difficult to comprehensively evaluate the model, it is essential to consider all the indices to give an inclusive conclusion of the model performance. Taking all the indices into account, it is summarized that the ANN, SVM, ANFIS and M5P models are more effective and feasible than GEP and empirical models in characterizing the elastic modulus degradation, which also accords with the results in Fig. 20.

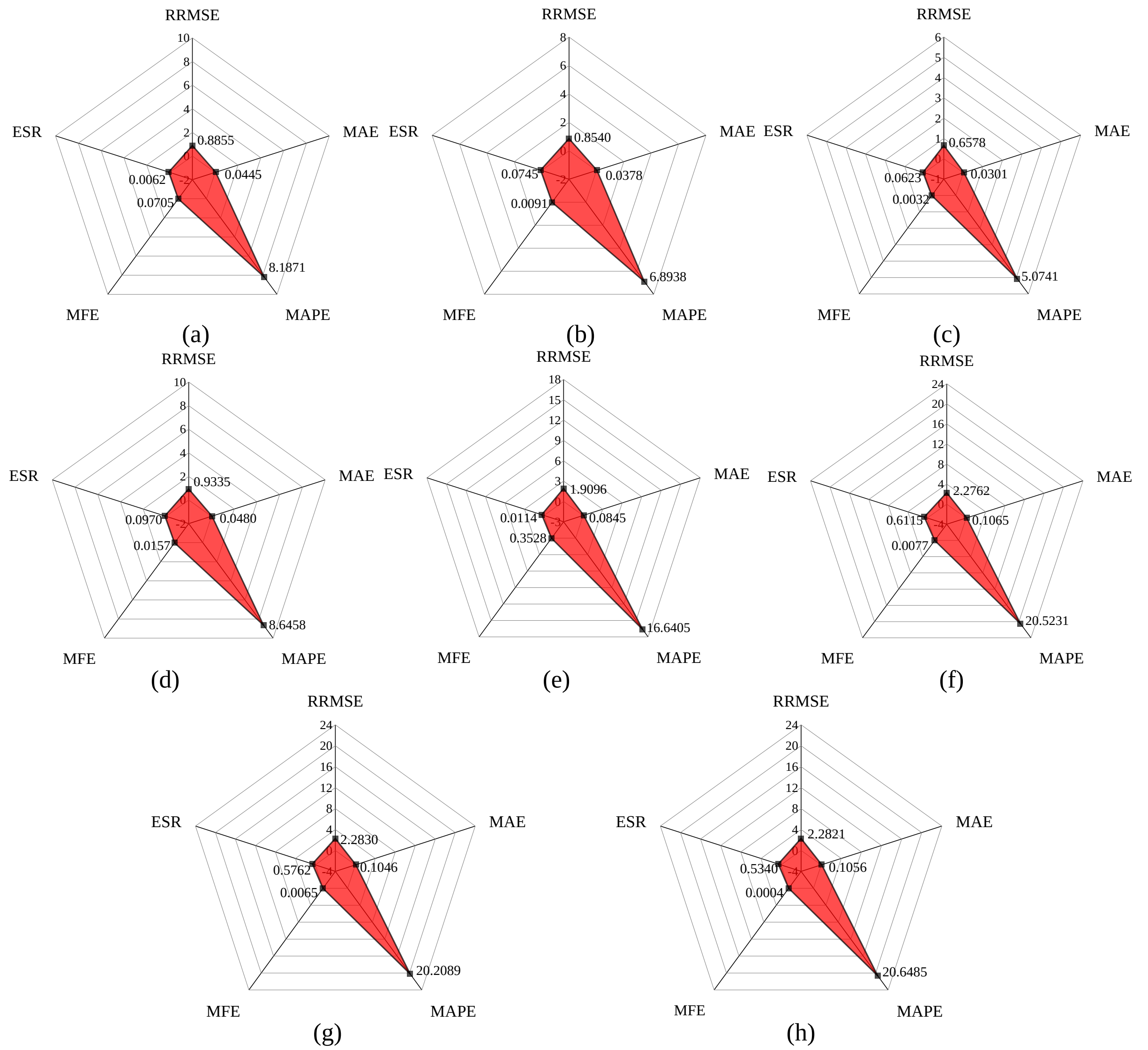

Fig. 21. Performance evaluation of eight models for predicting elastic modulus reduction, (a) ANN; (b) SVM; (c) ANFIS; (d) M5P; (e) GEP; (f) EM1; (g) EM2; (h) EM3.

4.3. Sensitivity analysis of input variables of SC models

To make full use of the developed SC models for predicting the elastic modulus of the ASR-affected concrete, a numerical study is conducted in this section to investigate the importance of each input parameter of the models on the model output (elastic modulus change). In this investigation, the reference values of input variables are defined as following: CC is 370 kg/m^3, WCR is 0.5, FRACR is 1, CRACR is 2, NRACR is 2, ET is 40 ºC, AC is 1.5%, CS is 35 MPa, CT is 14 days, MPE is 0.3%, and ME is 0.2%. For each input variable, its value is varied from 50% to 150% of the reference value (the change is from -50% to 50%) with the increment of 10%, while the values of other parameters are kept unchanged meanwhile. Then, the corresponding outputs of the SC models are recorded and the absolute values of relative error between model outputs and reference outputs are calculated as the indicator to analyse the sensitivity of each input variable. Eventually, the input variables are ranked according to the mean value of the relative errors of all the cases in the descending order. Fig. 22 and Table 7 display the results of sensitivity analysis of input variables of the SC models. In Fig. 22, the absolute values of relative errors corresponding to different inputs are portrayed by the spider chart, while the sensitivity ranking of these inputs is listed in Table 7. It is clearly seen that even though different SC models have certain deviations in the sensitivity ranking of input variables, the overall tendency of the ranking of these influencing factors can be guaranteed. Considering all the analysis results, it can be concluded that concrete content, exposure temperature and measured expansion are three most sensitive factors which are capable to significantly influence the elastic modulus of the ASR-affected concrete, and should be included in the model development. Conversely, the factors of ratio of fine reactive aggregate to cement, ratio of coarse reactive aggregate to cement and curing time have relatively less contributions to the elastic modulus prediction of ASR-affected concrete. Accordingly, these three parameters can be neglected in further model development and updating in the future work. The benefits of the sensitivity analysis of the influencing factors of SC models can be two-fold. First, fewer input variables indicate fewer measurements of the concrete specimens, which can effectively reduce the cost for elastic modulus evaluation of ASR-affected concrete and is much more convenient in the practical engineering application. Second, deleting insensitive variables can help to simplify the configuration of the SC models, which is able to avoid the over-fitting problem in model training and enhance the model accuracy using the limited data samples.

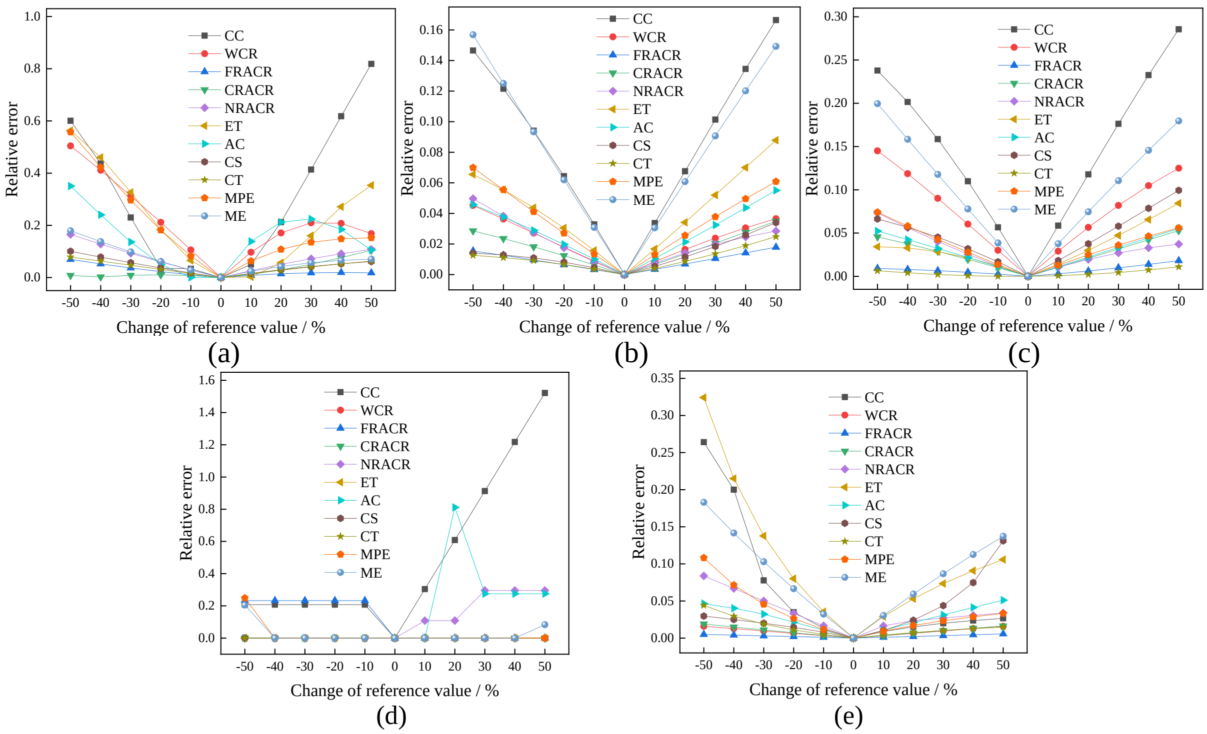

Fig. 22. Sensitivity analysis results of input variables of SC models, (a) ANN; (b) SVM; (c) ANFIS; (d) M5P; (e) GEP.

Table 7 Sensitivity ranking of input variables of SC models (MRE: mean relative errors)

ANN			SVM			ANFIS		
Input	MRE	Rank	Input	MRE	Rank	Input	MRE	Rank
CC	0.3136	1	CC	0.0875	1	CC	0.1487	1
WCR	0.2182	3	WCR	0.0228	6	WCR	0.0765	3
FRACR	0.0246	11	FRACR	0.0091	11	FRACR	0.0074	10
CRACR	0.0282	10	CRACR	0.0175	8	CRACR	0.0272	9
NRACR	0.0748	6	NRACR	0.0214	7	NRACR	0.0304	7
ET	0.2221	2	ET	0.0429	3	ET	0.0337	6
AC	0.1492	5	AC	0.0277	5	AC	0.0297	8
CS	0.0448	8	CS	0.0132	9	CS	0.0462	4
CT	0.0395	9	CT	0.0103	10	CT	0.0035	11
MPE	0.1953	4	MPE	0.0358	4	MPE	0.0357	5
ME	0.0695	7	ME	0.0836	2	ME	0.1036	2
M5P			GEP					
Input	MRE	Rank	Input	MRE	Rank			
CC	0.5092	1	CC	0.0622	3			
WCR	0.0000	7	WCR	0.0087	10			
FRACR	0.1059	3	FRACR	0.0029	11			
CRACR	0.0000	7	CRACR	0.0096	9			
NRACR	0.1004	4	NRACR	0.0348	4			
ET	0.0000	7	ET	0.1041	1			
AC	0.1489	2	AC	0.0278	7			
CS	0.0000	7	CS	0.0347	5			
CT	0.0000	7	CT	0.0143	8			
MPE	0.0226	6	MPE	0.0341	6			
ME	0.0262	5	ME	0.0866	2			

5. Graphical use interface (GUI) software design for predicting elastic modulus

In practice, the engineers may be not familiar with the theories of soft computing techniques and programming implementations. They are just terminal users to operate the models developed in this research. Therefore, in this regard, the user friendly software is designed for the engineers in the field, which compiles five SC models in a GUI. The whole software is composed of two interfaces, i.e. Login interface and Main interface, which are shown in Fig. 23. In the Login interface, the information of username and password is required before the engineer can utilize this software to evaluate the elastic modulus deterioration of concrete due to ASR. In the Main interface, the users can easily set the values of model inputs via the scroll bars and five trained SC models are available to be selected as the predictive tool for the elastic modulus evaluation. For the simplicity and convenient application, an executable file is generated from the codes developed on the platform of MATLAB, which can be detached from the MATLAB environment. An example is displayed in Figure 23 (b) for the purpose of software clarification. In this case, the values of cement content, water-to-cement ratio, coarse reactive aggregate to cement ratio, fine reactive aggregate to cement ratio, non-reactive aggregate to cement ratio, exposure temperature, alkali content, compressive strength, curing time, maximum measured expansion and measure expansion are 370 kg/m^3, 0.47, 0, 2.42, 2.78, 38 ℃, 1.25%, 36 MPa, 28 Days, 0.30%, 0.12%, respectively. The SVM model is selected and the prediction result is 0.5018. Currently, the software is just a preliminary version and the SC models are developed based on limited data samples with narrow ranges. In the future, more and more data samples collected in both laboratory and field, with wider ranges, will be employed to update the predictive models to improve their evaluation accuracies. Additionally, a new module will be included in the updated version to implement the online training of SC models.

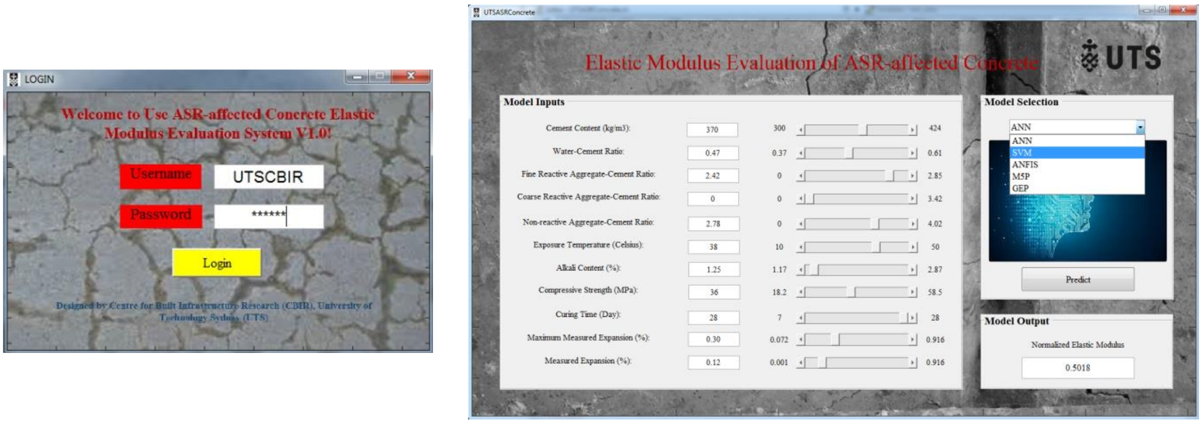

(a) (b)

Fig. 23. GUI for elastic modulus evaluation of ASR-affected concrete, (a) login interface; (b) main interface.

6. Conclusions

The influences of ASR on concrete mechanical properties, which can significantly impact serviceability and load-carrying capacity of ASR-affected concrete structures, are of high complexity. Existing models for evaluating degradations of concrete mechanical properties due to ASR suffer considerable inaccuracy in predicting modulus of elasticity for given level of expansion. This study aims at investigating the feasibility of using various soft computing techniques in evaluating the elastic modulus degradation of concrete affected by ASR. Five models, namely ANN, SVM, ANFIS, M5P and GEP, are developed based on a comprehensive data set. Their performances are compared to that of three commonly used empirical models in a wide range of evaluation indices. According to the investigation results, the following conclusions could be obtained:

(1) Compared to existing empirical models that only consider the expansion level as the variable, the proposed SC-based models have superior advantages on modelling the complexity of ASR affected concrete. It considers the ASR-induced expansion together with other influence factors such as cement content, water-to-cement ratio, coarse reactive aggregate to cement ratio, fine reactive aggregate to cement ratio, non-reactive aggregate to cement ratio, exposure temperature, alkali content, compressive strength and curing time, to produce comprehensive and realistic models and hence effectively enhance the evaluation accuracy.

(2) Through the comparison among five SC models and three empirical models, based on the absolute prediction error distribution and correlation coefficient between experimental and predicted results to evaluate the model capacity, it concludes that the ANFIS model offers the optimal capacity in estimating elastic modulus degradation.

(3) The proposed SC models also perform excellently against a wide range of statistic evaluation indices such as MSE, MAE, MAPE, MFE, ESR and RRMSE, which indicates the outstanding and robust abilities of proposed models and promising potentials for further practical application.

(4) Based on the developed SC models, the GUI software is developed using MATLAB platform to afford the structural engineer an easy and useful tool used in the field.

The finding of this study has offered different perspective for future study with SC models. For example, the hierarchy of the influencing parameters could be comprehensively investigated to understand the sensitivity associated with various input parameters for the modelling. In addition, relevant experimental studies are necessary to be conducted and the test results can enlarge the database for the model training, which can effectively improve the model accuracy and application range. Finally, it is important to note that the current form of SC models was developed for unrestrained concrete specimens. Therefore, improving the current form of SC models is necessary by considering the effect of confinement and/or reinforcement ratio to be applicable to the reinforced concrete, and further developing for different sets of input variables (i.e. measureable variables in the field) along with considering their time-dependency for the field concrete application.

Acknowledgement

The authors appreciate financial supports from Roads and Maritime Services as well as Australian Research Council via Nanocomm Hub (IH150100006).

References

[1] C. Giebson, K. Voland, H.M. Ludwig, B. Meng, Alkali-silica reaction performance testing of concrete considering external alkalis and preexisting microcracks, Struct. Concrete 18 (4) (2017) 528-538.

[2] L.F.M. Sanchez, B. Fournier, M. Jolin, J. Bastien, D. Mitchell, Practical use of the Stiffness Damage Test (SDT) for assessing damage in concrete infrastructure affected by alkali-silica reaction, Constr. Build. Mater. 125 (2016) 1178-1188.

[3] R. Hay, C.P. Ostertag, On utilization and mechanisms of waste aluminium in mitigating alkali-silica reaction (ASR) in concrete, J. Clean Prod. 212 (2019) 864-879.

[4] L.F.M. Sanchez, B. Fournier, M. Jolin, D. Mitchell, J. Bastien, Overall assessment of Alkali-Aggregate Reaction (AAR) in concretes presenting different strengths and incorporating a wide range of reactive aggregate types and natures, Cement Concrete Res. 93 (2017) 17-31.

[5] Y. Kubo, M. Nakata, Effect of reactive aggregate on mechanical properties of concrete affected by Alkali-Silica Reaction, in: Proceedings of 14th International conference on alkali-aggregate reaction (ICAAR). Texas, USA, 2012.

[6] G. Giaccio, R. Zerbino, J.M. Ponce, O.R. Batic, Mechanical behavior of concretes damaged by alkali-silica reaction, Cement Concrete Res. 38 (7) (2008) 993-1004.

[7] M.A. Getahun, S.M. Shitote, Z.C. Abiero Gariy, Artificial neural network based modelling approach for strength prediction of concrete incorporating agricultural and construction wastes, Constr. Build. Mater. 190 (2018) 517-525.

[8] Z.M. Yaseen, R.C. Deo, A. Hilal, A.M. Abd, L.C. Bueno, S. Salcedo-Sanz, M.L. Nehdi, Predicting compressive strength of lightweight foamed concrete using extreme learning machine model, Adv. Eng. Softw. 115 (2018) 112-125.

[9] M. Sonebi, A. Cevik, S. Grünewald, J. Walraven, Modelling the fresh properties of self-compacting concrete using support vector machine approach, Constr. Build. Mater. 106 (2016) 55-64.

[10] E. Sadrossadat, B. Ghorbani, M. Hamooni, M.H. Moradpoor Sheikhkanloo, Numerical formulation of confined compressive strength and strain of circular reinforced concrete columns using gene expression programming approach, Struct. Concrete 19 (3) (2018) 783-794.

[11] S. Jafari, S.S. Mahini, Lightweight concrete design using gene expression programing, Constr. Build. Mater. 129 (2017) 93-100.

[12] H. Basarir, M. Elchalakani, A. Karrech, The prediction of ultimate pure bending moment of concrete-filled steel tubes by adaptive neuro-fuzzy inference system (ANFIS), Neural Comput. Appl. 31 (2019) 1239-1252.

[13] A. Behnood, V. Behnood, M. Modiri Gharehveran, K.E. Alyamac, Prediction of the compressive strength of normal and high-performance concretes using M5P model tree algorithm, Constr. Build. Mater. 142 (2017) 199-207.

[14] A. Behnood, J. Olek, M.A. Glinicki, Predicting modulus elasticity of recycled aggregate concrete using M5′ model tree algorithm, Constr. Build. Mater. 94 (2015) 137-147.

[15] R. Esposito, C. Anaç, M.A.N. Hendriks, O. Çopuroglu, Influence of the alkali-silica reaction on the mechanical degradation of concrete, J. Mater. Civil Eng. 28 (6) (2016) 04016007.

[16] D.K. Bui, T. Nguyen, J.S. Chou, H. Nguyen-Xuan, T.D. Ngo, A modified firefly algorithm-artificial neural network expert system for predicting compressive and tensile strength of high-performance concrete, Constr. Build. Mater. 180 (2018) 320-333.

[17] A. Behnood, E.M. Golafshani, Predicting the compressive strength of silica fume concrete using hybrid artificial neural network with multi-objective grey wolves, J. Clean Prod. 202 (2018) 54-64.

[18] M. Sonebi, A. Cevik, S. Grünewald, J. Walraven, Modelling the fresh properties of self-compacting concrete using support vector machine approach, Constr. Build. Mater. 106 (2016) 55-64.

[19] A. Nazari, J.G. Sanjayan, Modelling of compressive strength of geopolymer paste, mortar and concrete by optimized support vector machine, Ceram. Int. 41 (9PartB) (2015) 12164-12177.

[20] M. Bilgehan, A.E. Kurtoğlu, ANFIS-based prediction of moment capacity of reinforced concrete slabs exposed to fire, Neural Comput. Appl. 27 (4) (2016) 869-881.

[21] E.K. Vahidi, M.M. Malekabadi, A. Rezaei, M.M. Roshani, G.H. Roshani, Modeling of mechanical properties of roller compacted concrete containing RHA using ANFIS, Comput. Concrete 19 (4) (2017) 435-442.

[22] J.R. Quinlan, Learning with continuous classes, in: Proceedings of the 5th Australian Joint Conference on Artificial Intelligence, 1992, pp. 343-348.

[23] J.R. Koza, Genetic programming as a means for programming computers by natural selection, Stat. Comput. 4 (2) (1994) 87-112.

[24] C. Ferreira, Gene expression programming: a new adaptive algorithm for solving problems, Complex Syst. 13 (2001) 87–129.

[25] S.M. Mousavi, P. Aminian, A.H. Gandomi, A.H. Alavi, H. Bolandi, A new predictive model for compressive strength of HPC using gene expression programming, Adv. Eng. Softw. 45 (1) (2018) 105-114.

[26] V. Saouma, L. Perotti, Constitutive model for alkali-aggregate reactions, ACI Mater. J. 103(3) (2006), 194–202.

[27] J.F. Seignol, N. Baghdadi, F. Toutlemonde, A macroscopic chemo-mechanical model aimed at re-assessment of delayed-ettringite-formation affected concrete structures, in: Proceedings of the 1st

international conference on computational technologies in concrete structures, Jeju, Korea, 2009, pp. 422-440.

[28] V. Sirivivatnanon, J. Mohammadi, W. South, Reliability of new Australian test methods in predicting alkali silica reaction of field concrete, Constr. Build. Mater. 126 (2016) 868-874.

[29] N. Smaoui, B. Bissonnette, M.A. Bérubé, B. Fournier, B. Durand, Mechanical properties of ASR-affected concrete containing fine or coarse reactive aggregates, J. ASTM Int. 3(3) (2005) 1-16.

[30] C. Larive, Apports combinés de l'expérimentation et de la modélisation à la compréhension de l'alcali-réaction et de ses effets mécaniques, École Nationale des Ponts et Chaussèes, Paris, 1997.

[31] B.P. Gautam, D.K. Panesar, S.A. Sheikh, F.J. Vecchio, Effect of coarse aggregate grading on the ASR expansion and damage of concrete, Cement Concrete Res. 95 (2017) 75-83.

[32] S. Multon, Evaluation expérimentale et théorique des effets mécaniques de l'alcali-réaction sur des structures modèles, Universitè de Marne-la-Vallèe (in collaboration with LCPCEDF), Champs sur Marne, 2003.

[33] M. Sargolzahi, S.A. Kodjo, P. Rivard, J. Rhazi, Effectiveness of nondestructive testing for the evaluation of alkali–silica reaction in concrete, Constr. Build. Mater. 24(8) (2010) 1398-1403.

[34] R. Pleau, M. Bérubé, M. Pigeon, B. Fournier, S. Raphaël, Mechanical behaviour of concrete affected by ASR, 8th International Conference on Alkali-Aggregate Reaction, Kyoto, Japan, 1989, pp. 721-726.

[35] T.U. Mohammed, H. Hamada, T. Yamaji, Relation between Strain on Surface and Strain over Embedded Steel Bars in ASR Affected Concrete Members, J. Adv. Concr. Technol. 1(1) (2003) 76-88.

[36] H. Kagimoto, Y. Yasuda, M. Kawamura, ASR expansion, expansive pressure and cracking in concrete prisms under various degrees of restraint, Cement Concrete Res. 59 (2014) 1-15.

[37] E.R. Giannini, Evaluation of concrete structures affected by alkali-silica reaction and delayed ettringite formation, University of Texas at Austin, 2012.

[38] L. Sanchez, B. Fournier, M. Jolin, J. Duchesne, Reliable quantification of AAR damage through assessment of the Damage Rating Index (DRI), Cement Concrete Res. 67 (2015) 74-92.

[39] Y. Zhuang, C. Qian, W. Xu, Alkali silica reaction expansion and mechanical properties of concrete containing glass aggregate with different sizes, Adv. Sci. Lett. 4 (4-5) (2011) 1611-1616.

[40] T.N. Nguyen, Y. Yu, J. Li, N. Gowripalan, V. Sirivivatnanon, Elastic modulus of ASR-affected concrete: An evaluation using Artificial Neural Network, Comput. Concrete 24 (6) (2019) 541-553.

[41] E.M. Golafshani, A. Behnood, Application of soft computing methods for predicting the elastic modulus of recycled aggregate concrete, J. Clean Prod. 176 (2018) 1163-1176.

[42] Y. Kawabata, J.F. Seignol, R.P. Martin, F. Toutlemonde, Kawabata, Y., Seignol, J.-F., Martin, R.-P., Toutlemonde, F., Macroscopic chemo-mechanical modeling of alkali-silica reaction of concrete under stresses, Constr. Build. Mater. 137 (2017) 234-245.

[43] R.P. Martin, L. Sanchez, B. Fournier, F. Toutlemonde, Evaluation of different techniques for the diagnosis & prognosis of Internal Swelling Reaction (ISR) mechanisms in concrete, Constr. Build. Mater. 156 (2017) 956-964.